鉛直下向き揚力を発生する没水翼の造波現象に関する研究

（研究課題番号　06452350）

平成７年度科学研究費補助金（一般研究（Ｂ））研究成果報告書

平成８年３月

研究代表者　茂里　一紘
（広島大学工学部教授）

はしがき

これまで、水中翼に関する研究は、水中翼船などの翼のように、鉛直上向きの揚力を発生させる翼に限られていた。本研究は、それとは全く逆の鉛直下向きの揚力を発生させる翼に着目するものである。研究代表者らは、これまで、翼付き半没型高速船の開発研究を進めてきた。これは、鉛直下向きに発生する揚力を利用して船を半没させることによって高速を実現しようとするものである。この研究の過程で、鉛直下向き揚力を発生する翼が静水中のみならず、波浪中においても抵抗を減少させることを発見した。

本研究では、鉛直下向き揚力を発生する翼は造波抵抗を軽減ないしはゼロにするという、これまで行なった実験結果の結論を境界要素法に基づく数値計算によって検証し、造波抵抗の主な発生場所である実用船型の船首近傍に鉛直下向き揚力を発生する翼を取り付けることによって、造波抵抗の軽減が実現できることを確認する。

研究組織

研究代表者	：	茂里一紘	(広島大学工学部教授)
研究分担者	：	土井康明	(広島大学工学部助教授)
研究分担者	：	二宮伸治	(広島大学工学部助手)

研究経費

平成６年度	４、４００千円
平成７年度	２、６００千円
計	７、０００千円

研究発表

(1) 学会誌等

Seung-Myun Hwangbo, Kazu-hiro Mori, Yasuaki Doi
Numerical Investigation on Wave Reduction by Wings Attached to Hull
Journal of the Society of Naval Architects of Japan, Vol.177 , pp.41-48 (1996)

研究成果

本研究では、まず、Tuckらが提唱した二次元波なし揚力体の理論を３次元流場に拡張した理論展開を行い、没水体の排水量分布に相当する鉛直下向き揚力を発生する特異点分布の波消し効果を検討した。

そして、翼付き没水船まわりの流れの計算に本研究で拡張改編した境界要素計算プログラムを適用して、翼の揚力変化が造波抵抗に及ぼす影響を調査し実験結果と比較検討した。境界要素法の計算には三角形パネル内で１次の内挿関数を用いて、速度ポテンシャルを求める直接法を用いた。翼後縁ではクッタの条件を満たすためのパネルを付加した。

翼形状およびアスペクト比や翼取り付け位置と主船体排水容積分布について検討し、鉛直下向きの揚力が造波抵抗を軽減させることを確認した。(1)

実用船型に取り付けた翼の造波抵抗軽減効果についても計算および実験により調査検討した。数値計算にはパネル内で２次の内挿関数を用いたランキンソース法を用い、翼は揚力線で近似した数値計算法を用いた。造波抵抗の計算には、表面圧力積分の数値誤差を避けるため、運動量積分による造波抵抗の計算法を提案した。まず計算法の妥当性を検討するため、シリーズ60船型および数種の実用コンテナ船型について実験から得られた波高、造波抵抗を計算結果と比較し、本数値計算の有用性を確めた。また、船首水面下に平板翼を取り付けた場合の波形計測結果と比較し、揚力線による翼の近似が妥当であることを確認した。

続いて、翼の位置と揚力の大きさが波と造波抵抗に及ぼす影響を調査し、鉛直下向きの揚力を発生する翼が造波抵抗を軽減させること、そして船体の適切な位置に翼を設置することにより、造波抵抗を効果的に軽減させることを確認した。また、波の山が位置する船首・船尾端近傍では鉛直上向きの揚力を発生する翼が造波抵抗を軽減することが判明した。(2)

本研究では、翼を主船体に取り付けることにより造波抵抗を軽減させるを確認したが、翼接続部の抵抗は無視できない量と考えられる。今後、主船体と一体化させた没水揚力体の可能性を検討することが望まれる。

（1）　下向き揚力を発生する翼を持つ没水船の造波抵抗について

1．　緒　言

次世代の高速船として茂里ら[1]は翼付き半没高速船（High Speed Semi-Submersible Vehicle with Wings = HSV）の研究・開発を行ってきた。このHSVは主船体に取り付けられた翼が発生する下向きに作用する揚力（即ち通常の水中翼とは逆向きに取り付けられており、この下向き揚力を以後負揚力と呼ぶ）によって主船体を没水させて造波抵抗を軽減し高速走行を実現する排水量型の船舶である。このHSVの流体力計測を行ったところ、主船体に翼を取り付けた場合と翼無しの場合では翼がある場合の方が造波抵抗が小さくなることが分かった。また翼が発生する揚力が大きくなるに従って造波抵抗が小さくなるという傾向も見られた。この事実はHSVにとって非常に有利な特性であるので、この現象を負揚力のを発生する翼の波消し効果と考え、より好ましい翼を求めるためにさまざまな翼形状について数値シミュレーションを行った。

2.　翼の波消し効果

スケールモデルによる流体力計測の結果をFig.　1に示す。これを見るとFnが大きい領域で翼有りの場合の方が翼無しのものより抵抗が小さくなっているのが分かる。またこの造波抵抗の結果を見てみると翼有りの場合の造波抵抗がかなり小さいものであることが判る。このことから船体と翼が造る波とが干渉して造波が抑えられていると推測される。そこでこの現象を説明するために *Tuck*[3]によって提唱されている "Waveless submerged lifting body" の考えを導入した。

三次元の*Laplace*方程式の解を考える。

$$\Phi(x,y,z) = D(x,y,z+h) - D(x,y,z-h) - \kappa[V(x,y,z+h) - V(x,y,z-h)]$$

ここでκは線形自由表面条件

$$\kappa = \Phi_z + \Phi_{xx}$$

であり、$D(x,y,z)$と$V(x,y,z)$はそれぞれ原点に置かれたdipoleとvortexで

$$D(x,y,z) = xr^{-3}$$

$$V(x,y,z) = -\frac{z}{r(r-x)}$$

となりそれぞれ自由表面条件をみたす。

このΦがつくる流場のポテンシャルは

$$\phi = Ux + \frac{1}{4\pi}\int S(\xi)\Phi(x-\xi,y,z)d\xi$$

で表される。ここで$S(\xi)$はdipoleが発生する船体の横断面面積である。

またvortexが発生する揚力は

$$L = -\rho g\int S(x)dx$$

となり船体に働く浮力と等しい大きさとなる。ここで$V(x,y,z)$を$S(\xi)$に比例する適切なものを選ぶと波を発生しない。

3.　シミュレーション結果

3.1　低アスペクト比の翼によるシミュレーション

上述の理論に従って船体の横断面に比例したvortexを想定して翼弦長の長い翼について計算した。各翼形状のパラメータと造波抵抗と揚力の無次元値をTable　1　に、翼形状をFig. 1 に示す。翼形状を決定するにあたり面積と前縁後退角、翼の取り付け位置は一定とし、断面形状はNACA4412とした。シミュレーション結果をTable2, Fig. 4 に示す。この結果を見ると翼弦

長が長くなることにより揚力がx方向に長く分布し造波抵抗が減るものと考えられたが、結果は逆のものになった。これは揚力の値を見ると翼弦長が長くなると揚力値が小さくなっているために、翼の波消し効果が小さくなり、結果として造波抵抗に差が出たものと考えられる。波消し効果を得るためには十分な揚力を発生するvortex、即ち翼である必要があるがこのケースではアスペクト比が小さい翼であるためにvortexの強さが十分でなかったといえる。また揚力の等高線を見ると翼前縁の最も大きく揚力を発生している部分は翼にほぼ直交している。これは揚力をx方向に分布させるという意味では適切とはいえないことになるであろう。さらに翼の中央付近の正の（上向きの）揚力を発生している部分が長く広範囲に分布しておりこれも波消し効果とは逆に作用していると考えられる。このケースでは翼弦長を長くして揚力を長く分布させるのが目的であったが翼面積の分布が必ずしも揚力の分布とはならないことが判った。

3.2 前縁後退角の違う翼によるシミュレーション

前述の結果をふまえて翼の前縁後退角を変化させたケースについてシミュレーションを行った。このケースの翼形状のパラメータをTable 3 に、パネル分布をFig. 5 に示す。このケースではある程度の揚力を得るために翼面積を先ほどのシリーズより大きくしたが、シリーズでは一定とし、翼取り付け部と翼端部での翼弦長は一定とした。このシリーズの造波抵抗及び揚力値をTable 4 に示す。前縁後退角の違いに対して揚力はほぼ一定の値となっているが造波抵抗の値は若干ではあるが減少する傾向が見られる。また揚力の分布と等高線をFig. 6 に示す。これから前縁後退角を与えることで揚力を長く分布させることができたといえるであろう。さきのケース1との比較では値そのものはそれほど小さいわけではないが翼面積が大きいことを考えると相対的には抵抗減であるといえる。

3.3 高アスペクト比の翼によるシミュレーション

大きな揚力を発生する高アスペクト比の翼が取り付けられた場合のケースについてシミュレーションを行った。翼形状のパラメータをTable 5 にパネル分布をFig. 7 に示す。このケースも翼面積と前縁後退角および取り付け位置を一定として翼のアスペクト比を変化させた。このケースのシミュレーション結果をTable6, Fig.8に示す。アスペクト比が高くなり揚力が大きくなるにつれて造波抵抗が小さくなることが判る。またこの造波抵抗の減少は主に翼の部分であるということも興味深い点である。

4. 結　言

負揚力を発生する翼の波消し効果を検証するためにさまざまな形状のシリーズについて数値シミュレーションを行った結果、以下のことが判った。アスペクト比の小さい翼について計算したところ揚力の値が小さくなったために造波抵抗は増加した。また翼の前縁後退角を変化させて計算した結果、後退角が大きくなるに従って造波抵抗が小さくなる傾向が得られた。前縁後退角により揚力をx方向に長く分布させることで波消し効果を強めることができるものと思われる。さらにアスペクト比の大きな翼について計算した結果アスペクト比が高くなり揚力が大きくなるに従って造波抵抗が減少する傾向が見られた。このことから揚力の大きさそのものも波消し効果を左右する重要な要素であるといえる。これらの結果から負揚力を発生する翼の波消し効果にどういった傾向があるかを知ることができた。

参考文献

[1] 茂里　一紘："A Study on Semi-Sbmersible High Speed Ship with Wings -Its Resistance Characteristics and Possibility-"; Journal of The Society of Naval Architects of Japan, Vol.164, Dec. 1988

[2] E.O.Tuck : "ASubmerged Body with Zero Wave REsistance"; Journal of Shio Reseach, Vol.33, No.2, pp.81-83, June 1989

[3] E.O.Tuck : "SUBMERGED BODIES THAT DO NOT GENERATE WAVES"; Abstrace for 7th International Workshop on Water Waves and Floating Bodies, May 1992

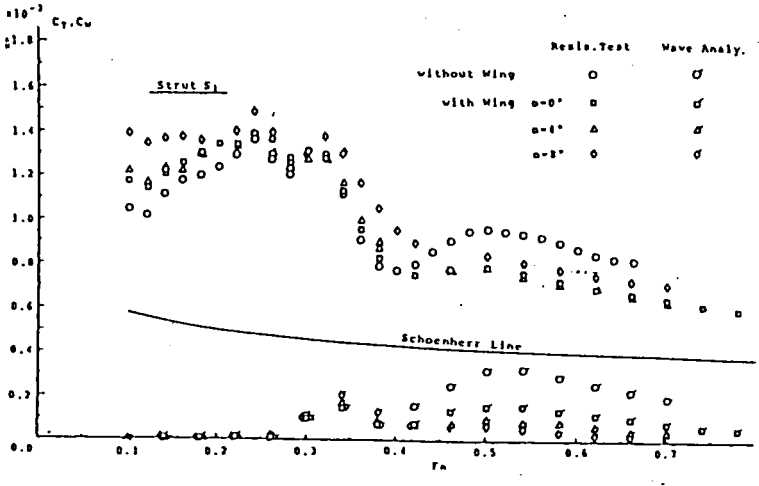

Fig. 1 Results of resistance test

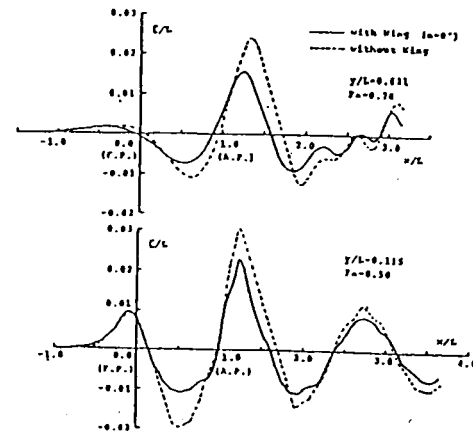

Fig. .2 Comparison of wave profile between with and without wing

Table 1 Parameters of wing figure : series 1

case	cdl-r	cdl-t	wing span	aspect ratio
1-a	0.125 L	0.103 L	0.110 L	0.88
1-b	0.150 L	0.132 L	0.090 L	0.60
1-c	0.175 L	0.160 L	0.075 L	0.43
1-d	0.200 L	0.187 L	0.067 L	0.34
1-e	0.225 L	0.213 L	0.060 L	0.27

cdl-r : chord length at wing root

cdl-t : chord length at wing tip

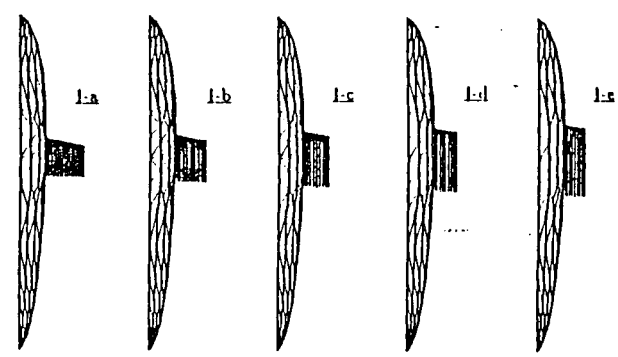

Fig. 3 Wing figures : series 1

Table 2 Results of computation : series 1

case	C_W ($\times 10^{-3}$)			C_L ($\times 10^{-3}$)
	Total	Body	Wing	
1-a	2.740	2.546	0.194	-2.078
1-b	2.835	2.650	0.185	-1.796
1-c	2.888	2.719	0.169	-1.463
1-d	2.982	2.784	0.198	-1.381
1-e	3.060	2.858	0.202	-1.243

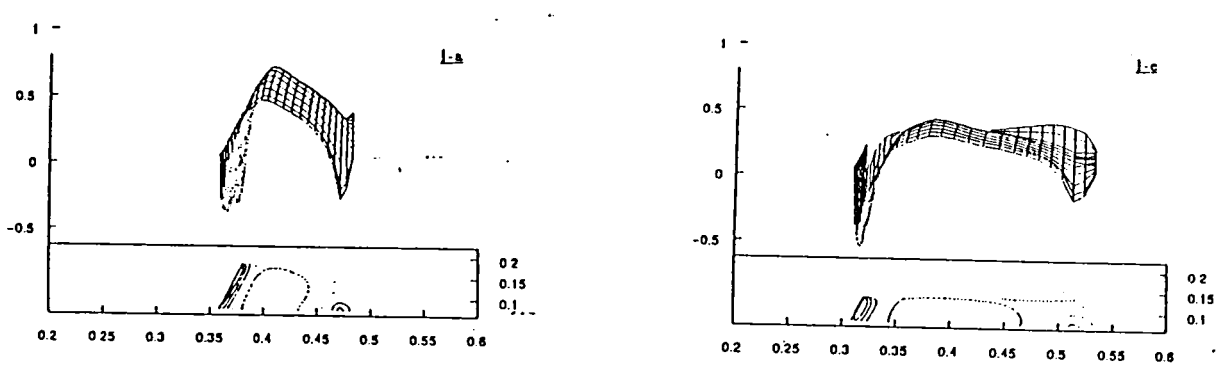

Fig. 4 Lifting force distribution on wing : series 1

Table 3 Parameters of wing figure : series 2

case	β (deg.)	cdl-r	cdl-t	wing span
2-a	10.0	0.20 L	0.10 L	0.10 L
2-b	20.0			
2-c	30.0			
2-d	57.3			

β : sweep back angle

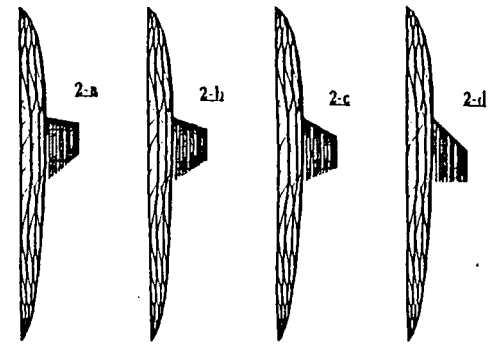

Fig. 5 Wing figures : series 2

Table 4 Results of computation : series 2

case	C_{IV} ($\times 10^{-3}$)			C_L ($\times 10^{-2}$)
	Total	Body	Wing	
3-a	2.925	2.692	0.232	-1.990
3-b	2.872	2.685	0.186	-2.026
3-c	2.809	2.676	0.134	-2.038
3-d	2.823	2.636	0.186	-2.030

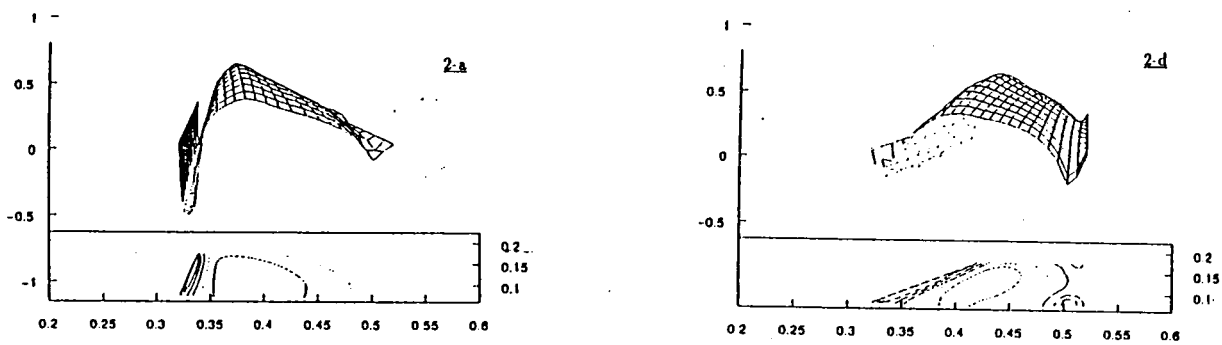

Fig. 6 Lifting force distribution on wing : series 2

Table 5 Parameters of wing figure : series 3

case	cdl-r	cdl-t	wing span	aspect ratio
3-a	0.090 L	0.063 L	0.167 L	1.81
3-b	0.085 L	0.059 L	0.175 L	1.95
3-c	0.080 L	0.056 L	0.188 L	2.35
3-d	0.075 L	0.053 L	0.200 L	2.67
3-e	0.100 L	0.070 L	0.150 L	1.50

cdl-r : chord length at wing root
cdl-t : chord length at wing tip

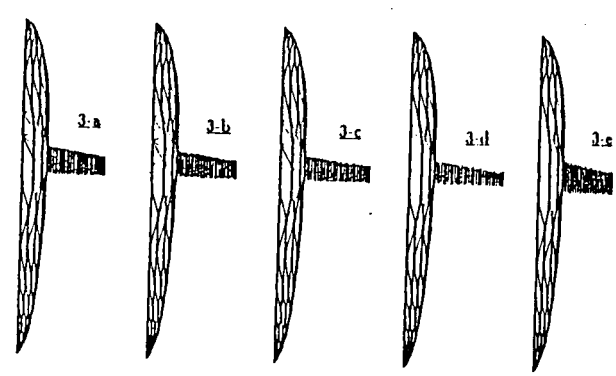

Fig. 7 Wing figures : series 3

Table 6 Results of computation : series 3

case	C_{IV} ($\times 10^{-3}$)			C_L ($\times 10^{-2}$)
	Total	Body	Wing	
2-a	2.630	2.313	0.318	-2.618
2-b	2.511	2.200	0.281	-2.696
2-c	2.353	2.244	0.109	-2.705
2-d	1.999	2.209	-0.210	-2.467

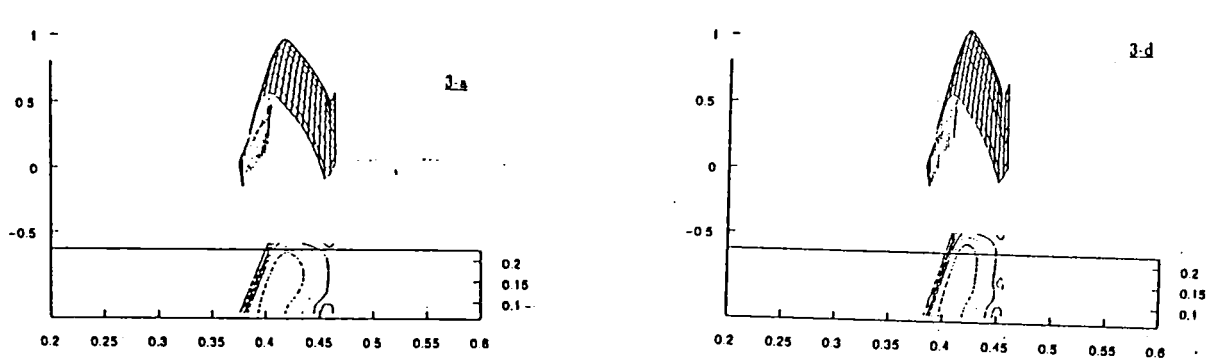

Fig. 8 Lifting force distribution on wing : series 3

（2） 船体に取り付けた翼による造波抵抗の軽減について

1 Introduction

Rankine source method was suggested as one of numerical tools to solve a boundary value problem on the basis of source distributions over a hull and free surface. It is well appreciated that the numerical treatments based on the Rankine source are simple and the results are quite acceptable. Dawson[2] have proposed the double model linearized free surface condition and the finite difference scheme to meet the radiation condition.

Based on the Dawson's proposal, Mori et al.[5),6)] have developed a modified Rankine source method, in which a higher order source distribution scheme was used, and have shown reasonable agreements with the experimental results for simple hull forms. Their method don't fully satisfy both the hull and free surface boundary conditions to save the computation time, so the application is very limited only to the simple hull forms.

In present paper we modified the method to satisfy the both boundary conditions with a iterative procedure. A new approach to use the double model flow velocity potential including the effect from the wavy velocity potential on the free surface during the iteration is adopted. The present method is computed and compared with various hull forms including the actual ship with high block coefficient. The agreement between the computation and the experiment shows the method is very useful even in a complicated hull form.

For the application of the Rankine source method, Many papers have been also introduced in the extensive range including unsteady ship motion problem[8),9)] as well as ship wave computations at high speed[1),3)] or under shallow water condition[11)]. A hydrofoil problem at high speed range[1),7)] is also solved by the Rankine source method.

As a further application to extend the utility of the Rankine source method, we carry out computations of flows and resistance of a single hull with a pair of wings generating lifting forces. In the computation, the wings are approximated by a lifting line and the induced velocities by this lifting line are conglomerated into the Rankine source method. By this approximation, the flow can be simply treated without any complicacies due to the Kutta condition and can be solved only to satisfy the body and free surface boundary conditions.

For the purpose of confirming the present computation, some model tests with or without wings are carried out. The agreement between computation and experiment confirmed that the wing can be replaced by the lifting line. Various computations are performed not only by changing the location, angle of attack and ship speed but also

with multiple vortices to investigate the wave phenomena and to analyze the mechanism of the wave interaction between the main hull and the attached wings. Through these calculations, we may expect a possibility to develop some appendages to reduce the wave resistance.

The present paper is consisting of six chapters. The modified Rankine source scheme adopted by the present study is outlined in chapter 2. Chapter 3 describes the computational method of wing approximation and a pilot calculation for its verification. Chapter 4 presents various wave simulations including the wave reduction on a ship with wings generating the various lifting forces. More precise experiments are carried out in the wide range of speed and are compared with the results of the calculation in chapter 6. New formula for wave resistance is also derived in terms of the Lagally theorem and added in appendix.

2 Modified Rankine Source Method

2.1 Basic equation

We assume that a ship is advancing with a constant speed U in a still water with infinite depth and width. The x-axis of the coordinate system is parallel to the direction of the uniform flow, while the y-axis and the z-axis to the direction of starboard side and to the upward direction respectively as shown in Fig.(2.1). The viscosity of the fluid is neglected.

The total velocity potential ϕ is expressed as follows.

$$\phi = \phi_o + \phi_w \tag{2.1}$$

where ϕ_o: double model flow velocity potential included the effect from wavy velocity potential and ϕ_w: wavy velocity potential. The total velocity potential ϕ satisfies the following equations;

o Laplace equation

$$\Delta\phi = 0 \quad in \quad fluid \quad domain \tag{2.2}$$

o Dynamic free surface boundary condition

$$g\zeta + \frac{1}{2}(\phi_x^2 + \phi_y^2 + \phi_z^2 - U^2) = 0 \quad (z = \zeta) \tag{2.3}$$

where ζ : wave height and g : acceleration of gravity. Subscripts mean the differentiation with respect to the referred variable.

o Kinemàtic free surface boundary condition

$$\phi_x\zeta_x + \phi_y\zeta_y - \phi_z = 0 \quad (z = \zeta) \tag{2.4}$$

o Hull boundary condition

$$\phi_n = 0 \quad on \quad hull \quad boundary \tag{2.5}$$

o Radiation condition

$$\nabla\phi = (U, 0, 0) \quad at \quad x \to -\infty \tag{2.6}$$

After linearization of the two free surface conditions, we get a following double-hull linearized free surface boundary condition.

$$\phi_{ol}^2\phi_{wll} + 2\phi_{ol}\phi_{oll}\phi_{wl} + g\phi_{wz} = -\phi_{ol}^2\phi_{oll} \quad (z = 0) \tag{2.7}$$

where l : streamline direction. A four-point upstream finite difference scheme proposed by Dawson[2] is employed to satisfy the radiation condition.

The problem is to satisfy the hull boundary condition of Eq.(2.5) and the free surface boundary condition of Eq.(2.7) at the same time. Once the total velocity potential is determined, the wave elevation ζ is calculated by Eq.(2.3).

The pressure on the hull surface can be derived from Bernoulli's theorem.

$$p = -\rho g z + \frac{1}{2}\rho(U^2 - \nabla\phi^2) \tag{2.8}$$

where z : vertical distance from free surface.
Wave resistance can be calculated by integrating the above pressure components in streamwise direction over the hull surface panels.

$$R_w = -\int\int_{S_H} p n_x ds \tag{2.9}$$

where S_H : hull surface and n_x : x-component of the outer normal to panel surface.

The wave making resistance is usually calculated by the above pressure integration over the body. However, this sometimes brings forth significant errors due to the complicacies of body geometries or sharp change of pressure. The pressure change is expected to be large in the present study because the pair of line vortices is placed close to the body. This demerit of the pressure integration can be made innocent by adopting a very small panel, which requires large computer capacity and computing time. Alternatively, we use here an expression of the wave resistance derived in terms of the Lagally theorem(see Appendix for the details);

$$R_w = R_{wo} + 2\pi\rho\int\int_{S_F} u'\sigma_F ds + \rho\int\int\int_V (w\omega_y - v\omega_z)dV \tag{2.10}$$

$$R_{wo} = \frac{1}{2}\rho\int_{-\infty}^{+\infty} dy \int_{-\infty}^{0} (\phi_y^2 + \phi_z^2 - \phi_x^2)dz + \frac{1}{2}\rho g\int_{-\infty}^{+\infty}\zeta^2 dy \tag{2.11}$$

where u, v, w : components of velocity, $\omega_x, \omega_y, \omega_z$: components of vorticity, u' : u excluding the contribution of σ_F at the integrating position and σ_F : source distribution on the free surface(S_F). The first term of the formula is the linear component and the second term is the additional component due to the singularities on the free surface and the last is the contribution of the inviscid vorticity.

2.2 Numerical treatment

The hull and free surfaces are divided into several panels. Sources are placed on the panels. Source densities are calculated to satisfy the aforementioned hull and free surface boundary conditions. All values are non-dimensionalized by the half of ship length. The extension of the calculating domain in the streamwise direction is from -2 $\sim$ -1.5 (from F.P.) to 2.0 $\sim$ 2.5 (from A.P.) based on Froude number and the domain in transverse direction is from 0 (centreline) to 0.75. At least 15 grids over the free surface along streamwise direction are placed per one wave length ($\lambda_o = 4\pi Fn^2$).

A higher order source distribution in streamwise and transverse directions is adopted for the free surface panels to increase the accuracy of the calculation.

$$\sigma_w = \sigma_0 + \sigma_1 s + \sigma_2 s^2 + \sigma_3 st + \sigma_4 l + \sigma_5 l^2 \tag{2.12}$$

The surrounding 6 points are used to describe the one free surface source density. It was referred from Mori et al.[5] that this higher approximation for the discrete source density shows good agreements with the experimental results for the simple hull forms even if the added velocity term on the hull panel due to the wavy velocity potentials is ignored.

For the general purpose of the program, the present computation was extended to solve the both hull and free surface boundary conditions by iterative scheme. The iterative procedure can save both computing time and memory storage in comparison with the full matrix solving.

The flow computation proceeds through the following sequence of steps;

- Inputting the hull offsets data.

- Preprocess for calculation.
  - Hull panel rearrangements based on equal girth space division.
  - Free surface panel generation based on Froude number.

- Hess and Smith method calculation without free surface ($\phi_w = 0$).
  - Calculation of the double model velocity potential ϕ_o, in which the Froude number term is not included(Fn=0), by solving the following equation;

$$\frac{\partial \phi_o}{\partial x} n_x + \frac{\partial \phi_o}{\partial y} n_y + \frac{\partial \phi_o}{\partial z} n_z = 0 \tag{2.13}$$

  - Calculation of induced velocity ϕ_{ol} on the free surface panel by the double model flow velocity potential.

- Wavy velocity potential ϕ_w calculation on the free surface.
  - $-\phi_{ol}^2 \phi_{oll}$ calculation by using 5-points central finite difference scheme.(right-hand side of Eq.(2.7))

- $\phi_{ol}^2\phi_{wll} + 2\phi_{ol}\phi_{oll}\phi_{wl} + g\phi_{wz}$ calculation by using 4-points upstream finite difference method.(left-hand side of Eq.(2.7))
- Wavy velocity potential ϕ_w can be obtained by solving the Eq.(2.7).
- Calculation of the induced velocity (V_x, V_y, V_z) on the hull panel by the wavy velocity potential ϕ_w on the free surface.

- Recalculation of the Hess and Smith method including the induced velocity by the wavy velocity potential(Froude number term).
  - Calculation of new double model velocity potential ϕ_o with the Froude number term by solving the following equation;

$$(\frac{\partial\phi_o}{\partial x} + V_x)n_x + (\frac{\partial\phi_o}{\partial y} + V_y)n_y + (\frac{\partial\phi_o}{\partial z} + V_z)n_z = 0 \qquad (2.14)$$

- Calculation of new wavy velocity potential ϕ_w based on the new double model velocity potential.

- Final ϕ_o and ϕ_w will be obtained with iterative procedure.

- Wave resistance and wave profile can be calculated.

2.3 Computation results

Based on the modified scheme of the Rankine source method with the iterative procedure, we carry out computations for the various hull forms ranging from a simple hull to an actual full ship. The scheme is widely investigated with the various computations and their comparison with the experimental data. It can be concluded that the modified Rankine source method is very useful to compute and analyze the wave phenomena not only for the actual hull form but also for the local modification of the hull form. Followings are the detail descriptions of the compuatation results for the three various hull forms.

2.3.1 Series 60

First we carried out computations for the Series 60 to verify the present scheme. The hull form, wave profiles, wave contours, wave patterns and pressure contours over the hull surface for Fn=0.16, 0.25, 0.316, 0.35 are presented in Figs.(2.2) $\sim$ (2.6), respectively. The results for the wave resistance computation are presented in Fig.(2.7). The wave profile, wave contour and the wave resistance are compared with those of experiments. The agreement is fairy good over all ranges in wave profile. The computed and measured wave contour at Fn=0.316 shown in Fig.(2.4) also have a very similar pattern.

For wave resistance, we can conclude that the computation is acceptable except around the Froude number 0.33 in which a hollow is appearing too deeply in comparison with the measured results.

2.3.2 Container ships with bulbous bow

To verify the calculation for an actual hull form with a bulbous bow, two container hull forms that are slightly different only at the far forward parts were calculated. Figs.(2.8) $\sim$ (2.11) show the hull forms, wave profiles, wave patterns and pressure contours on the hull surface for the two containers respectively. The comparisons with the experimental results show that the wave profiles of the both hull forms have same patterns with those of the experiments over all the ranges even if the wave heights are still quite different at the far forward parts of the hulls.

Fig.(2.12) shows the wave resistance curves measured at Hyundai Model Basin from Fn=0.14 to 0.28 for the both hull forms. The wave resistance computed by the Lagally theorem are shown in Fig.(2.13). The comparisons indicate that the wave resistance of the base hull form is well agreed with the experiment over all the ranges but that of the revised hull form is a little different even if the total tendency is quite similar.

If we consider that the modification on the revised hull is very limited within the far forward local parts of the forebody, the computation result of the wave resistance may be more reasonable than that of the experiment. The wave resistances of the measurement were obtained on the basis of form factor anaysis, so they may be very sensitive and are likely leaded to a wrong result due to the false decision of the form factor. It's also abnormal that the difference in the wave resistances at the very slow Fn, where almost no wave resistance is normally expected, is too dominant in the experimental results.

Table.(2.1) Principal dimensions of two containers

ship particulars	
Length between perpendiculars	282.0 m
Breadth	32.25 m
draft	16.50 m
Block coefficient	abt. 0.63
LCB	abt. 5.9 m(A)
Design Speed	25.0 Knots
Froude number	0.244

2.3.3 Full ship with large block coefficient

We also carried out the calculation for a full ship having large block coefficient(Cb=0.8), very small L/B ratio(L/B=5.15) and very large B/d ratio(B/d=3.95). The ship has a bulbous bow, a stern bulb and a transom stern. Figs.(2.14) $\sim$ (2.16) show the hull form, wave profile and wave pattern respectively. Fig.(2.17) shows the wave resistance for very low speed from Fn=0.1 to 0.18. The results show that Cw value is negative over the very low Fn regions, which is normal in the Rankine source method using a coarse panels, and is too steeply increasing at the high Fn regions. Anyhow, it is probably reasonable in the range of design speed(Fn=0.16).

Table.(2.2) Principal dimensions of full ship

ship particulars	
Length between perpendiculars	235.0 m
Breadth	45.64 m
draft	11.58 m
Block coefficient	abt. 0.80
LCB	abt. 8.3 m(F)
Design Speed	15.0 Knots
Froude number	0.16

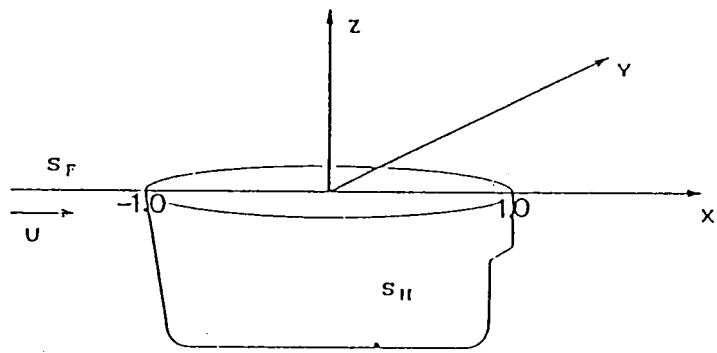

Fig.(2.1) Coordinate system

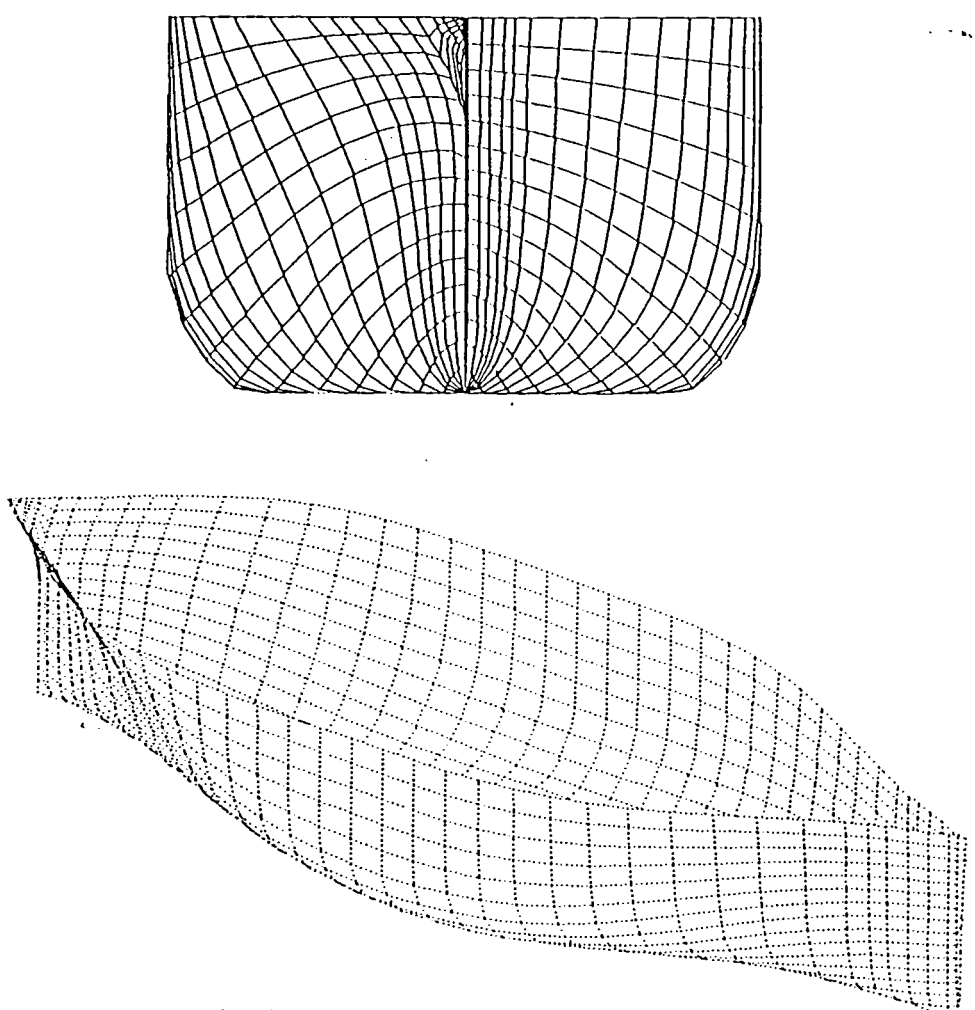

Fig.(2.2) Series 60(Cb=0.6) hull form

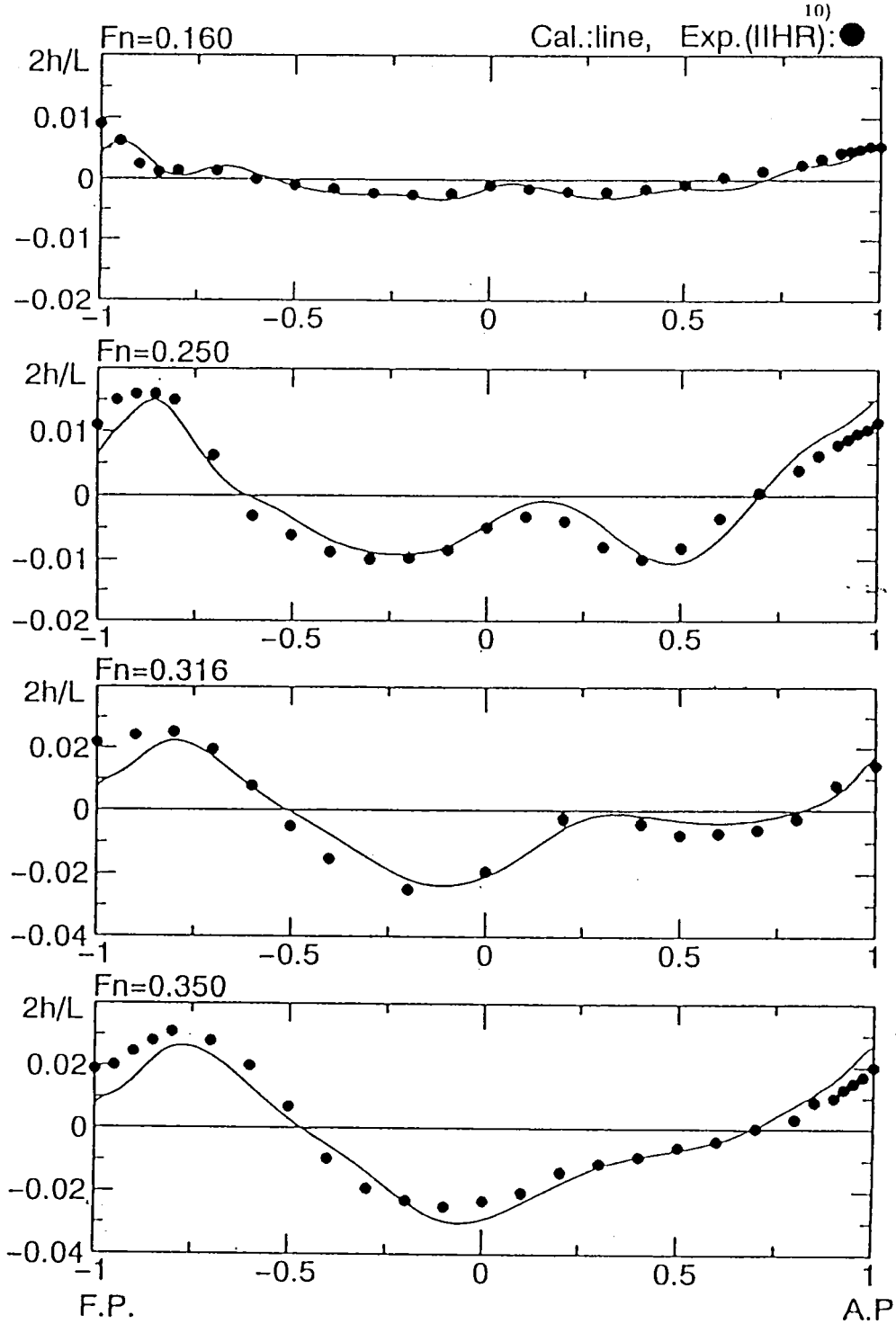

Fig.(2.3) Comparison of computed and measured wave profiles of Series 60

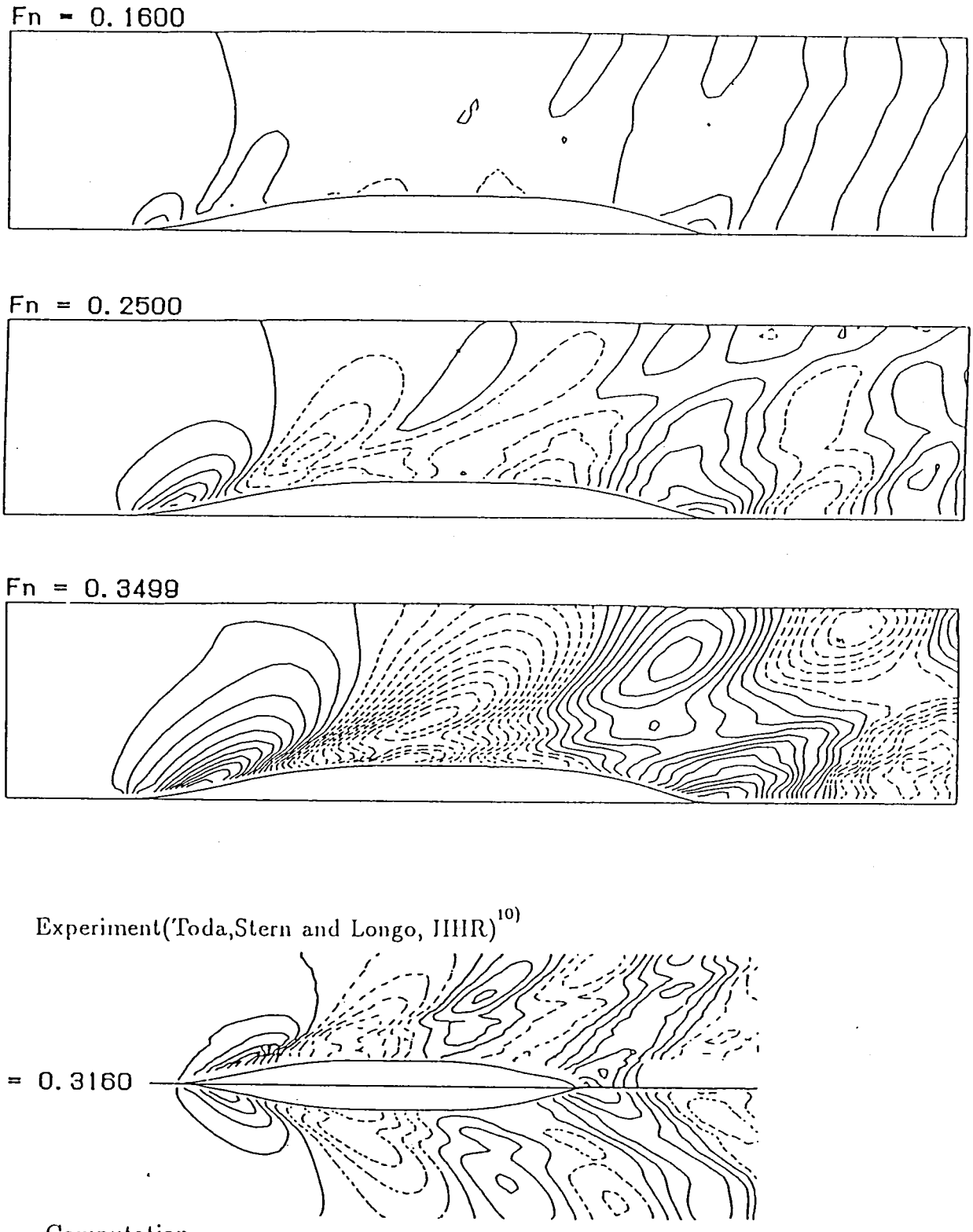

Fig.(2.4) Comparison of computed and measured wave contours of Series 60

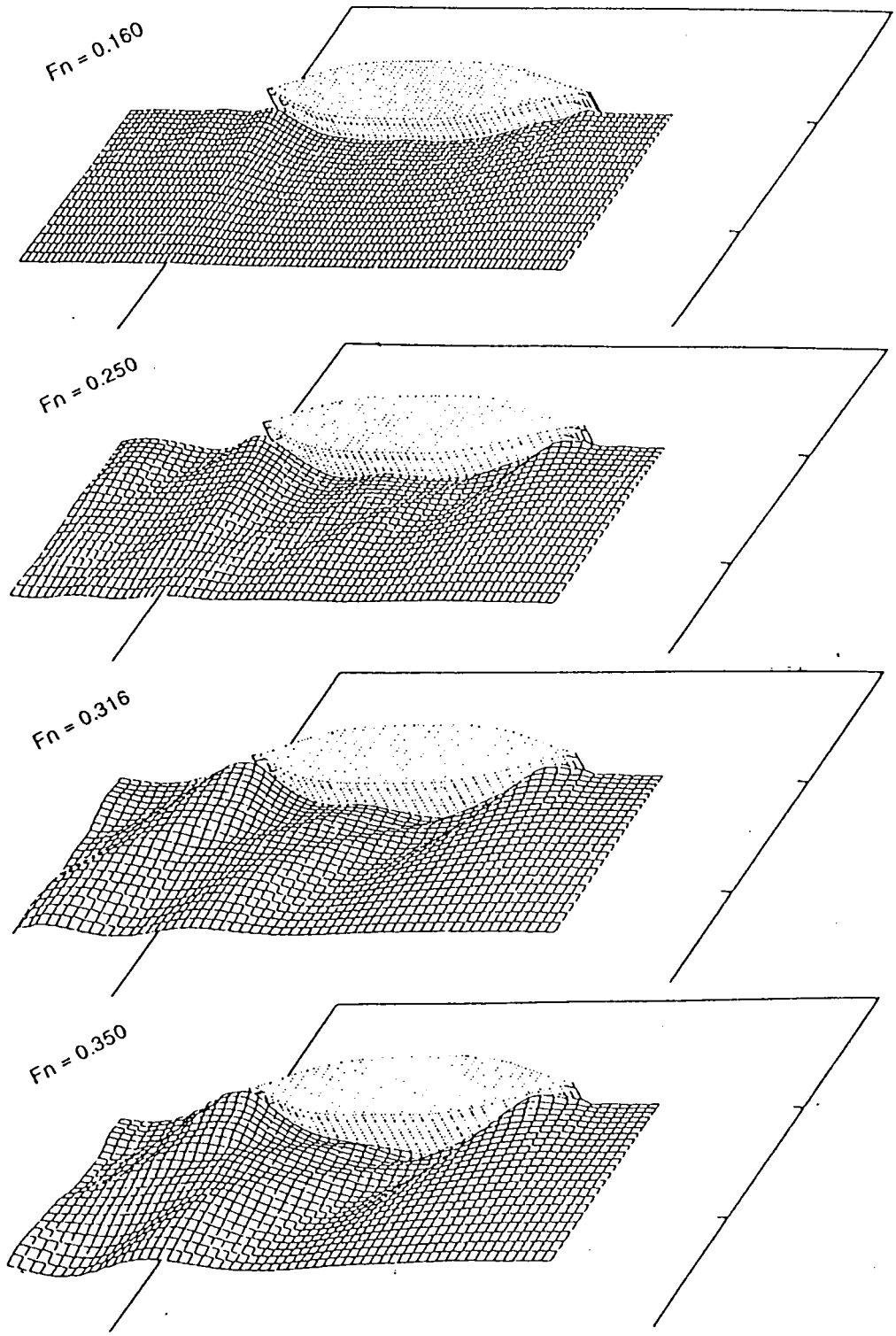

Fig.(2.5) Computed wave patterns of Series 60

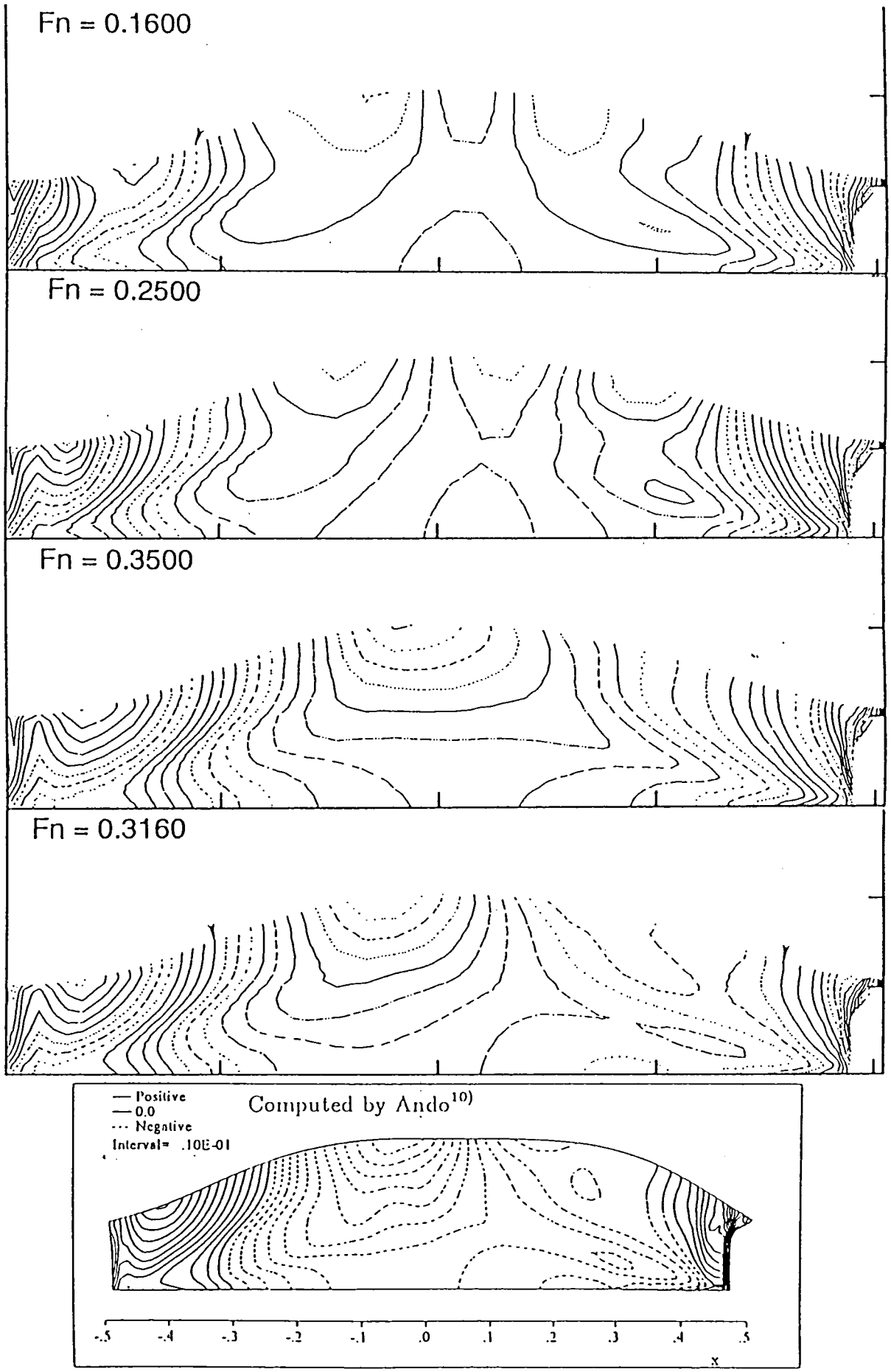

Fig.(2.6) Computed pressure contours of Series 60

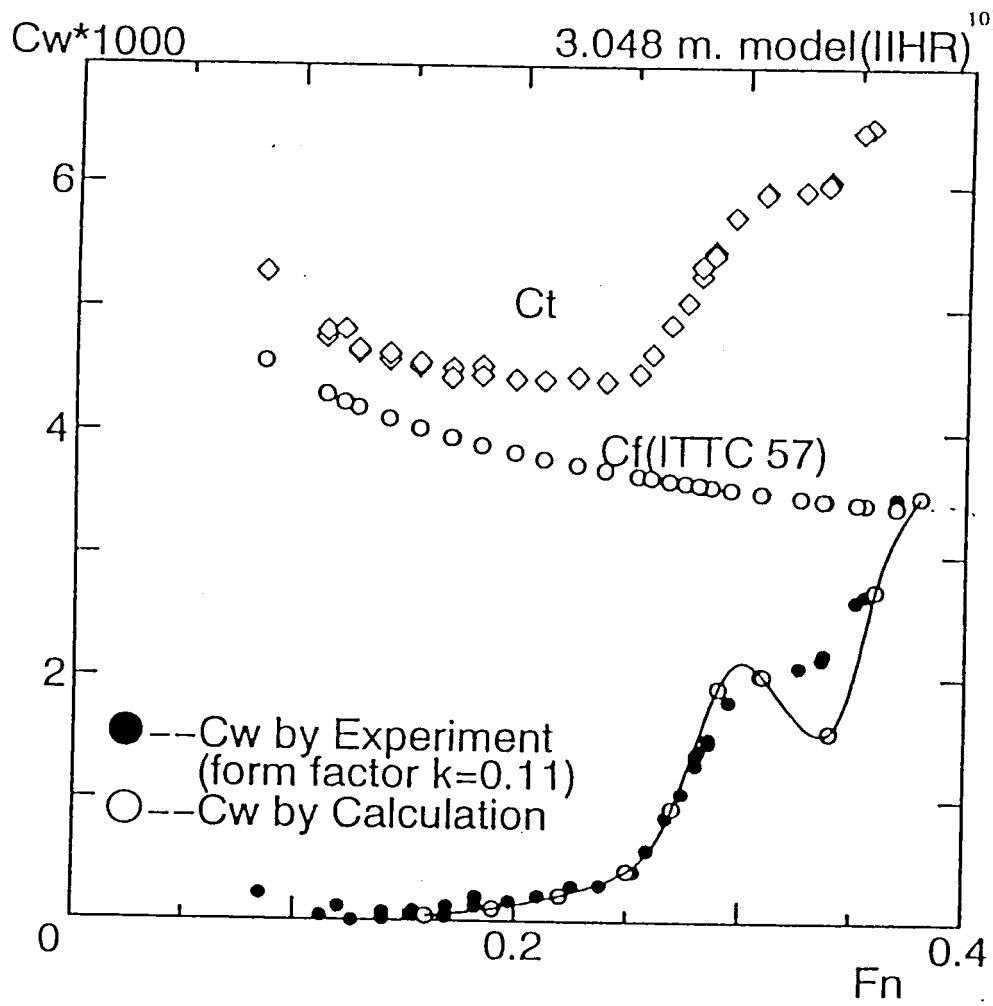

Fig.(2.7) Comparison of wave resistances of Series 60

Original

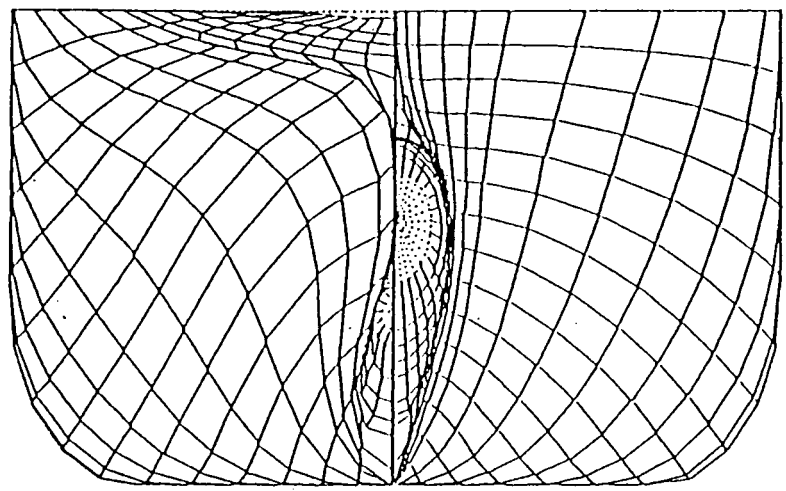

Revised

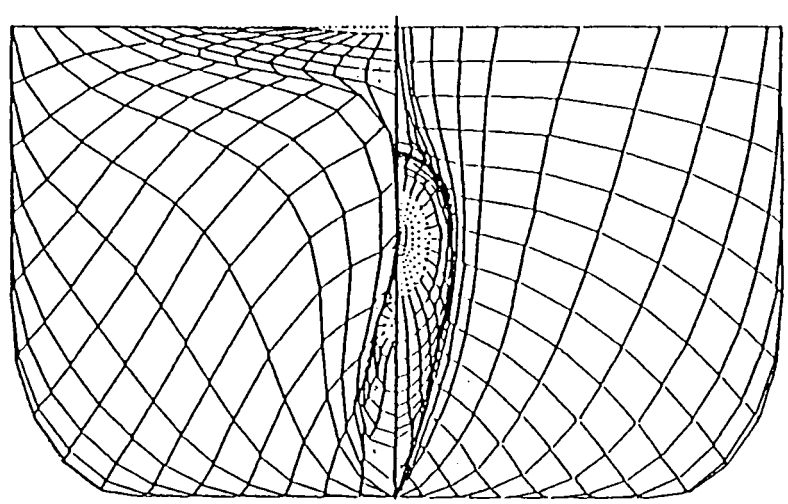

Fig.(2.8) Comparison of two container hull forms

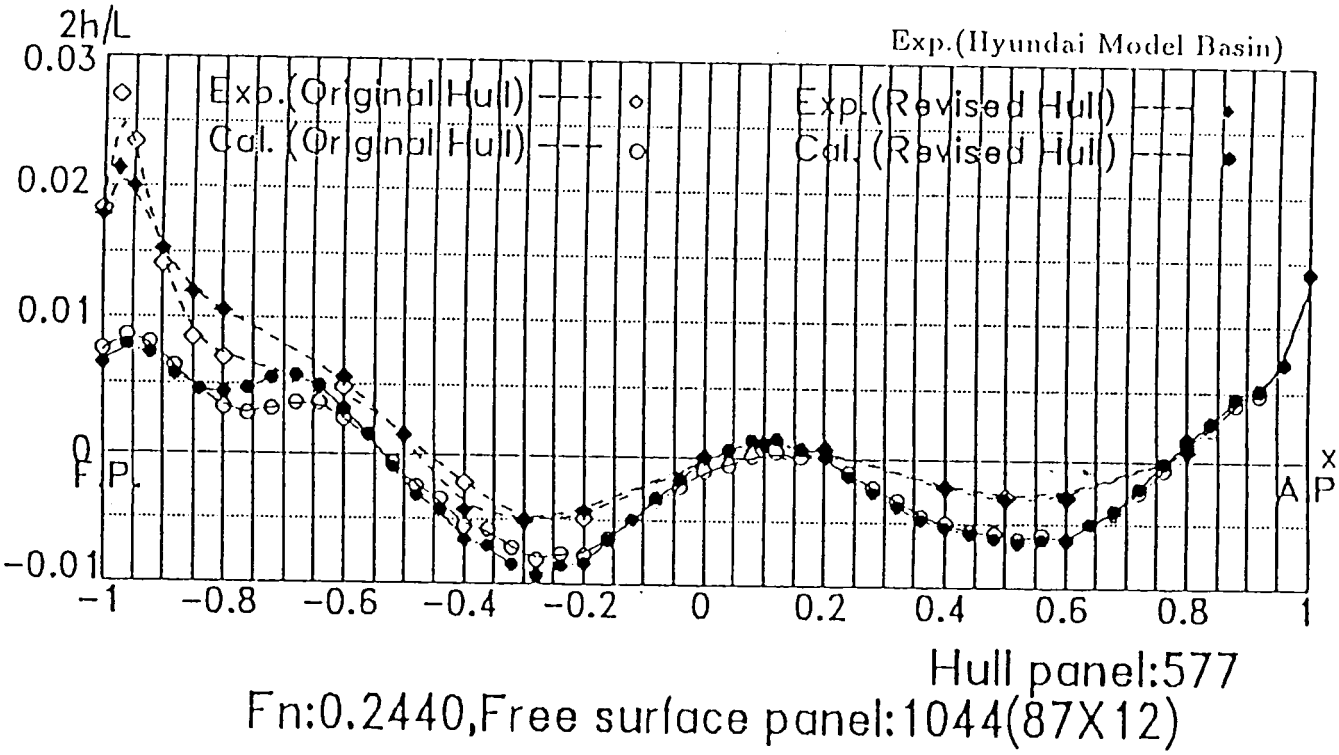

Fig.(2.9) Comparison of computed and measured wave profiles of two containers

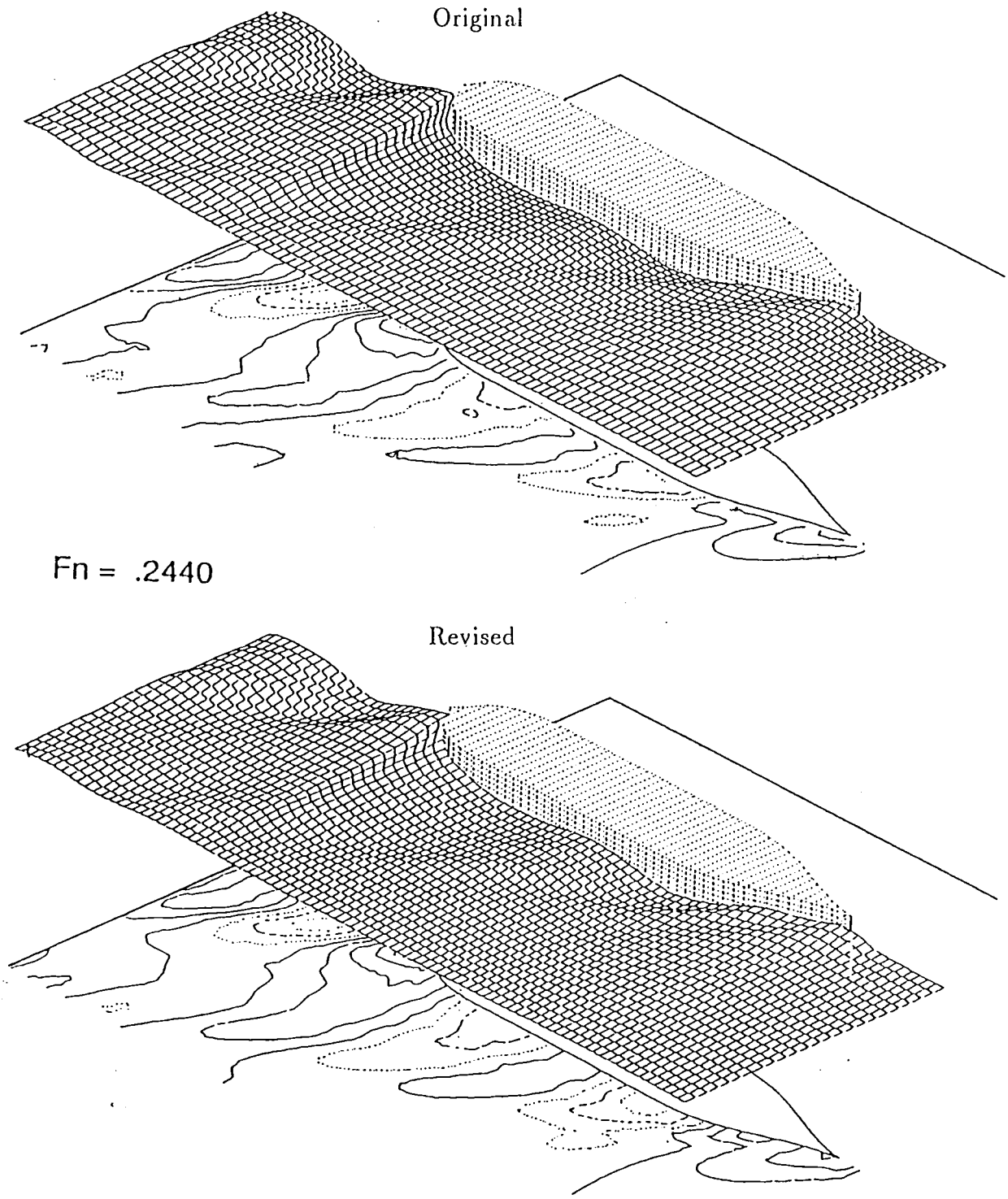

Fig.(2.10) Computed wave patterns of two containers(Fn=0.244)

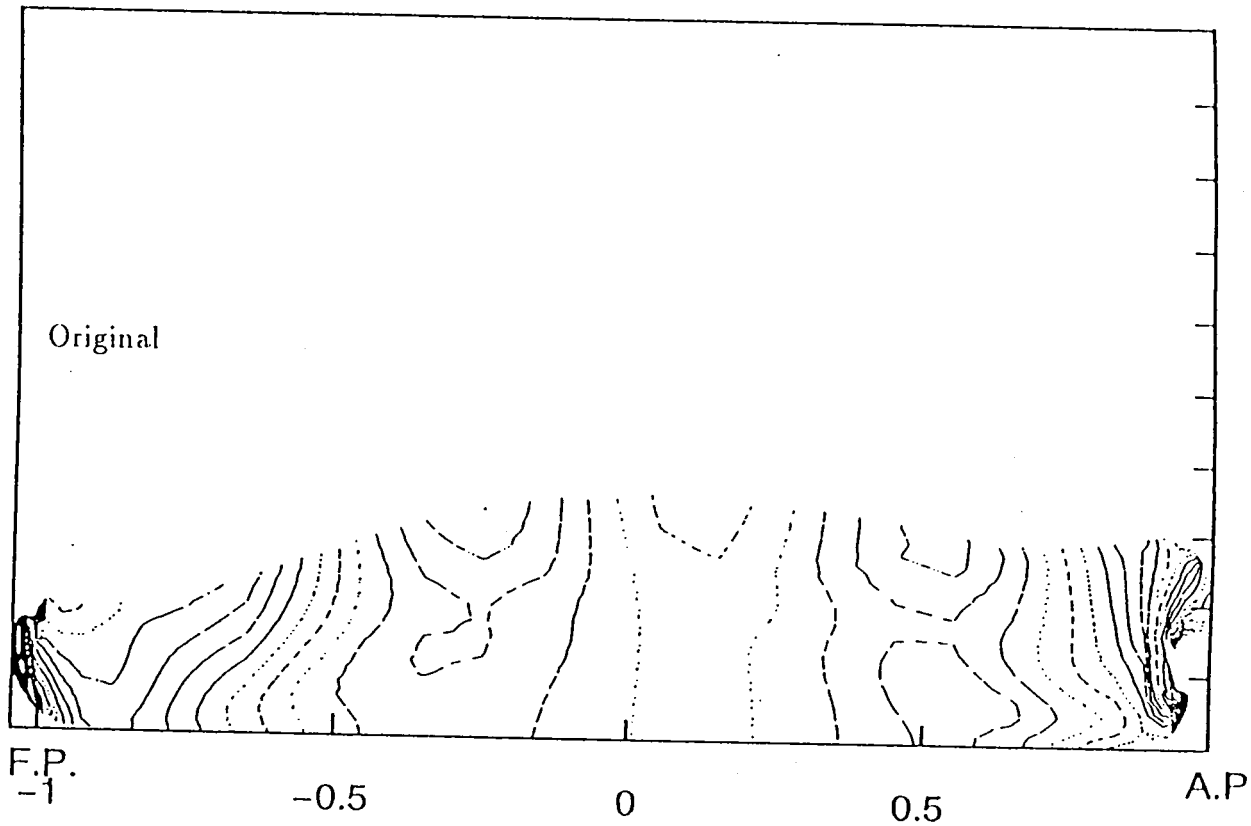

Fn = 0.2440

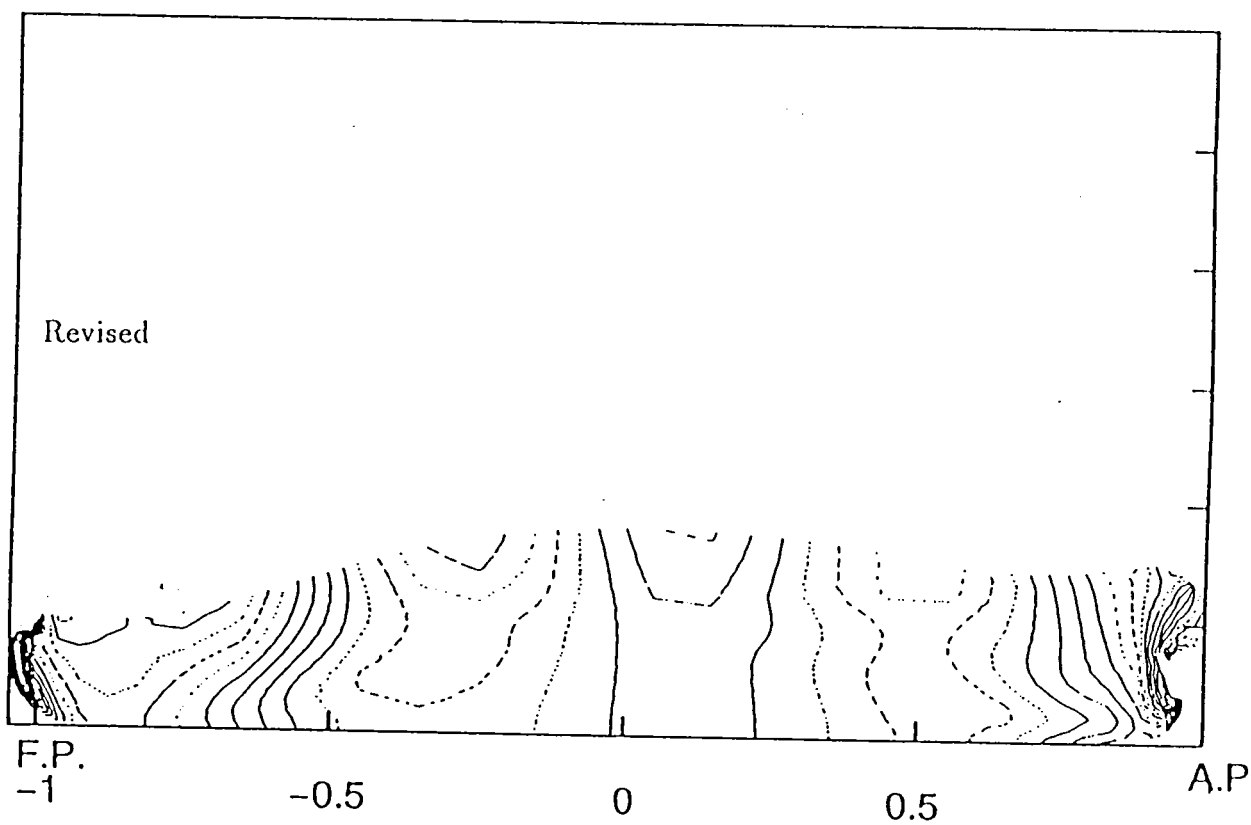

Fig.(2.11) Computed pressure contours of two containers(Fn=0.244)

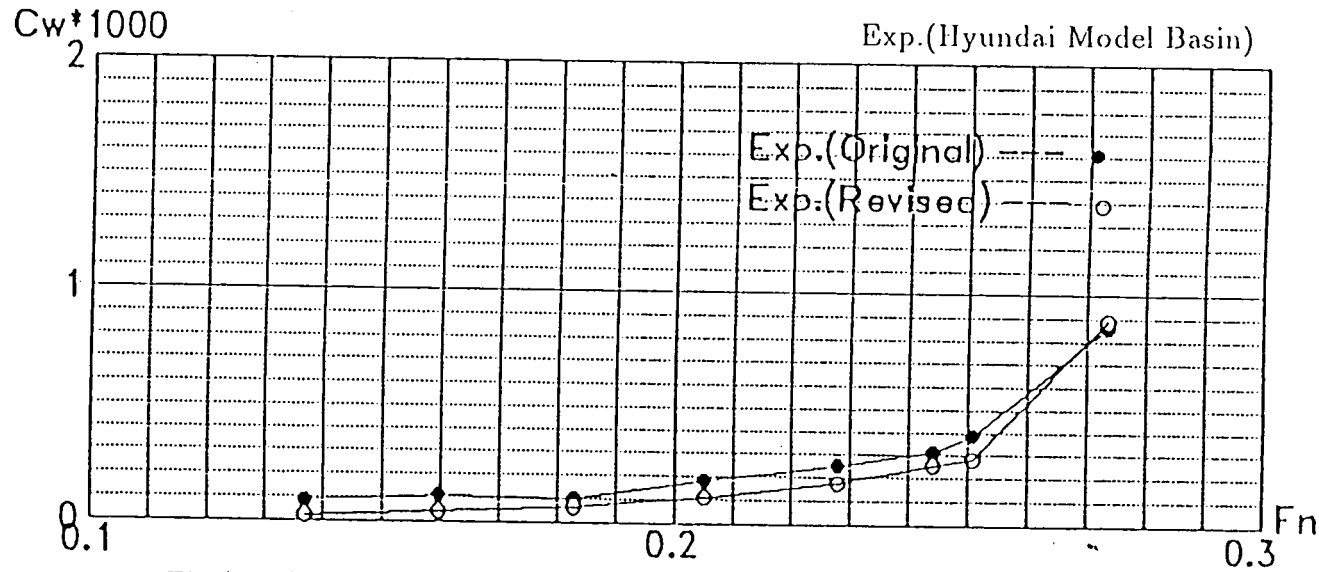

Fig.(2.12) Comparison of wave resistances of two containers(measured)

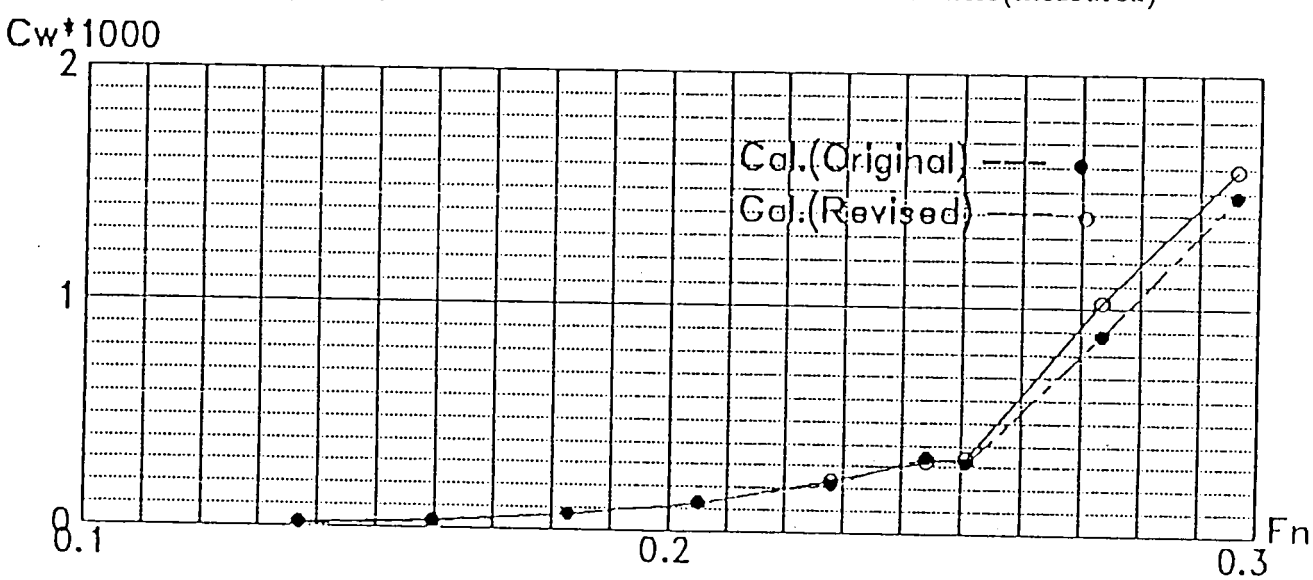

Fig.(2.13) Comparison of wave resistances of two containers(computed)

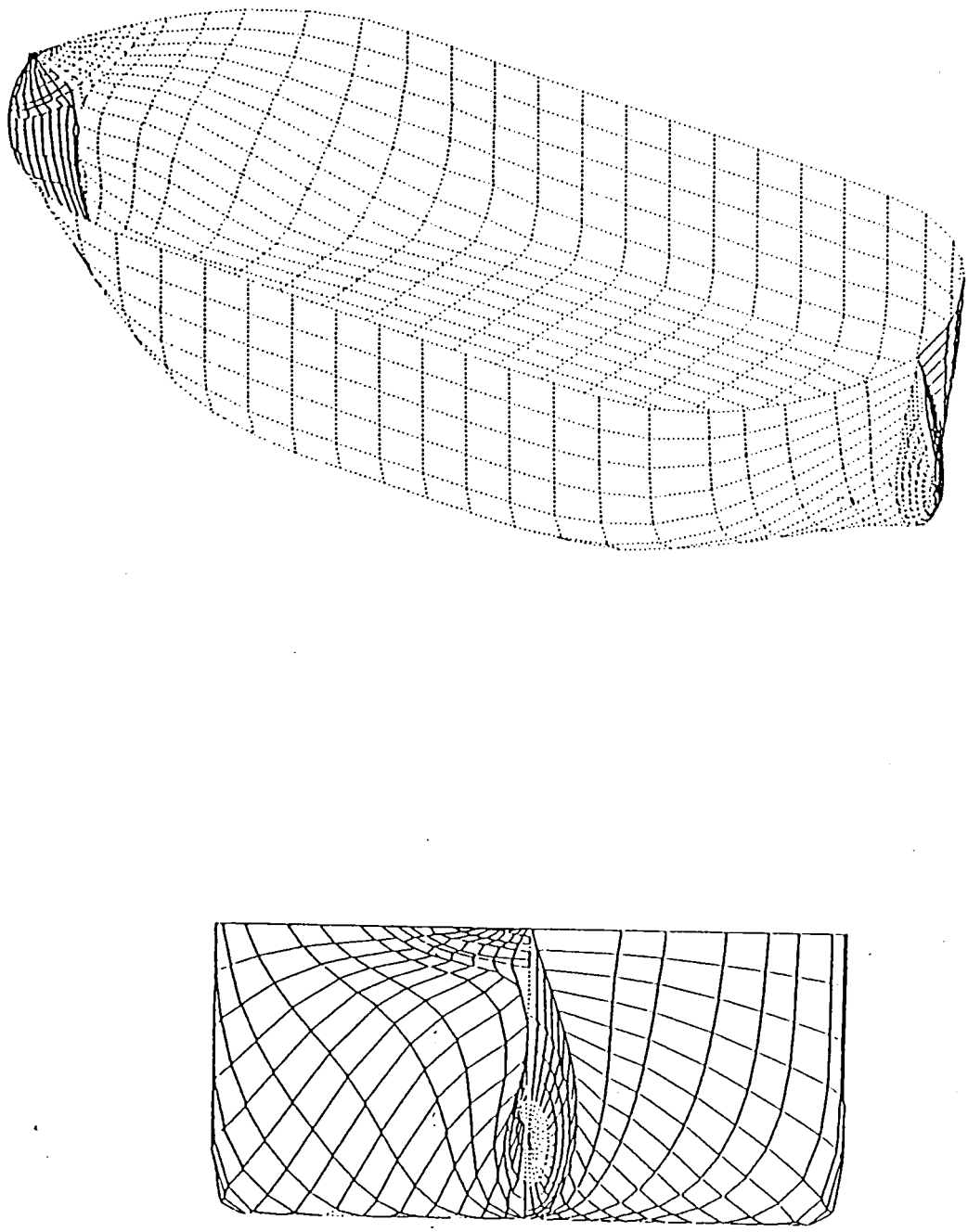

Fig.(2.14) Full ship hull form

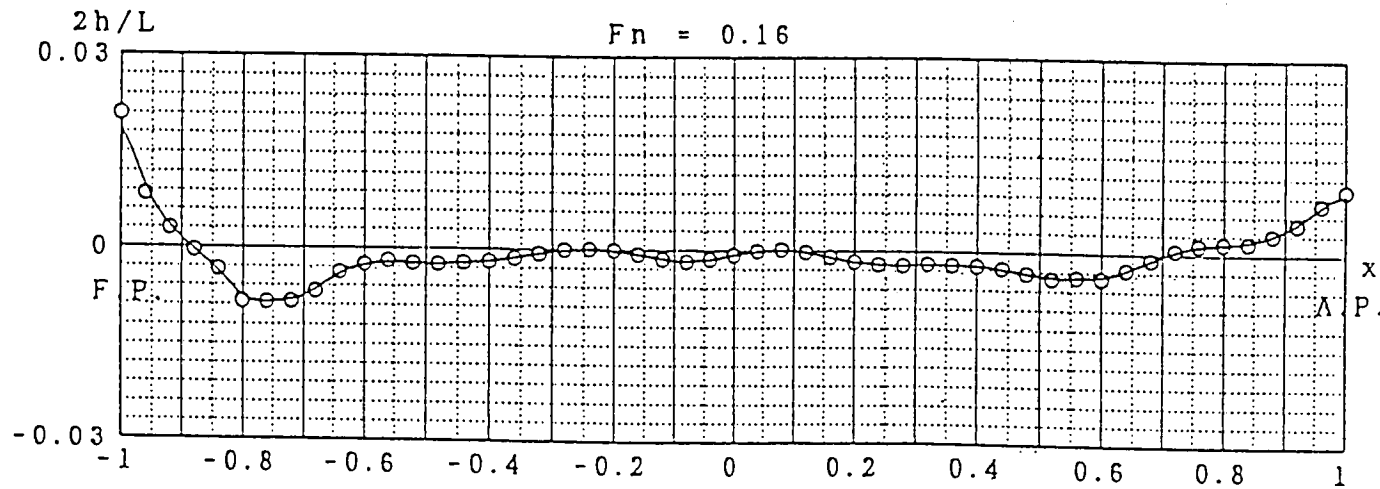

Fig.(2.15) Computed wave profile of full ship(Fn=0.16)

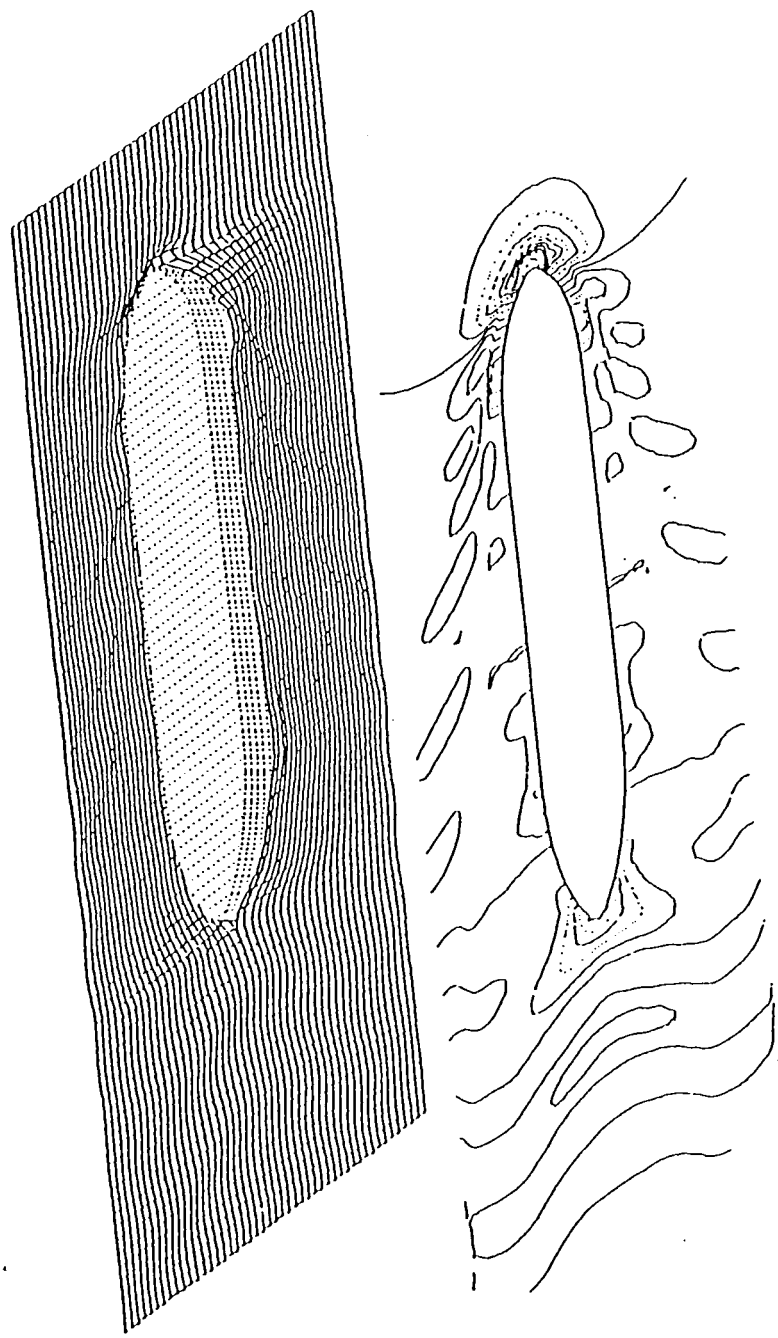

Fig.(2.16) Computed wave pattern of full ship(Fn=0.16)

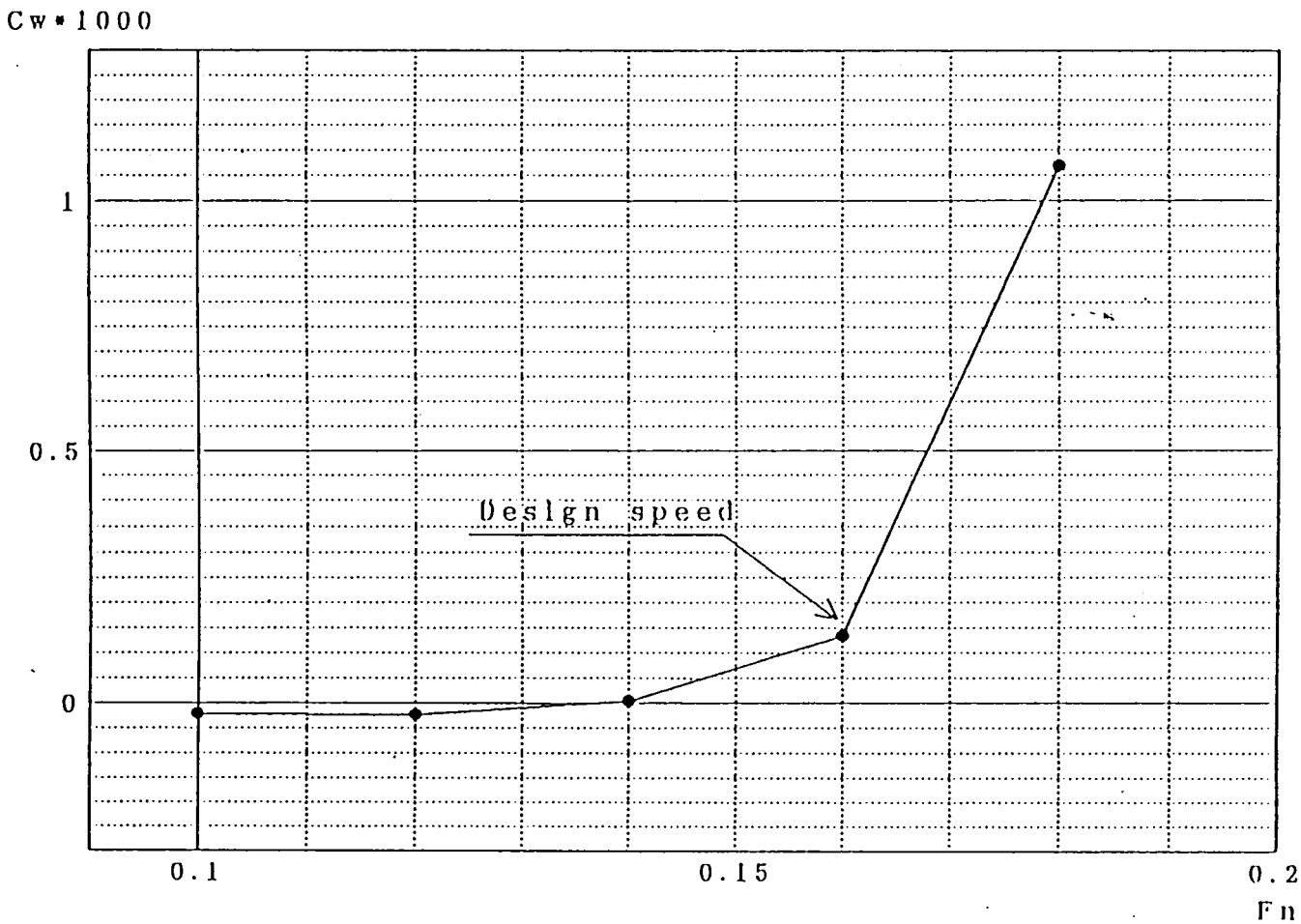

Fig.(2.17) Computed wave resistance of full ship

3 Computational Method for the Flow around a Hull with Wings

3.1 Lifting line approximation

The wing is simplified by a straight line vortex and the circulation on the wing associated with the lift is replaced by a vortex filament on the basis of lifting line theory. This vortex filament, so called line vortex, lies along the straight line whose strength is proportional to the local intensity of the lift. In our computation, we arrange a pair of line vortices on the hull side as shown in Fig.(3.1). The circulation distribution Γ is zero at each end and constant at middle part as presented in Fig.(3.2). The line vortices are assumed to start from just outside of the hull surface, which means they are not in contact with the hull.

The induced velocity v by the bound vortex is given by Biot-Savart law as follows;

$$v = \frac{1}{4\pi}\int rot(\frac{\Gamma(y')}{r}dy') = -\frac{1}{4\pi}\int \frac{r}{r^3}\times\Gamma(y')dy' \tag{3.1}$$

where r : distance vector. The drag by the vortex, corresponding to the third term of Eq.(2.10), is given by

$$D = \rho\int w(y')\Gamma(y')dy' \tag{3.2}$$

where $w(y')$ is the vertical velocity component on the line vortex.

The Eq.(3.2) can be replaced with two parts based on their derivations as follows;

$$\begin{aligned} D = \quad & \rho\int(w_{\phi_o}+w_{\phi_w})\Gamma(y')dy' \\ + \quad & \rho\int w_{downwash}\Gamma(y')dy' \end{aligned} \tag{3.3}$$

where w_{ϕ_o} : vertical velocity component due to double model flow velocity potential, w_{ϕ_w} : vertical velocity component due to wavy velocity potential and $w_{downwash}$: induced vertical velocity component by the trailing vortex of the line vortex. We computed the vertical velocity component of $(w_{\phi_o}+w_{\phi_w})$ for the case of a constant circulation distribution over all line vortex with B/2 span and a trailing vortex at the

tip of the span(x=-0.9). The results are presented in Fig.(3.3). The direction of the vertical component is upward, so this component contributes to lessen the resistance, which means thrust force as shown in Fig.(3.4). The amount of the thrust force by these two velocity potentials will be about 7% in comparison with the original wave resistance value of no wings at Fn=0.35.

The effects by the trailing vortex shedding from the line vortex are also generally important to simulate the 3-dimensionality of wing. The induced drag caused by this trailing vortex can be described in the second term of the above Eq.(3.3). Expected induced drag due to the downwash by the trailing vortex can be estimated by an approximation formula of $C_{Di} = \frac{C_L^2}{\pi\lambda}$ with assumption of an elliptical circulation distribution. The calculation shows the increment of the wave resistance will be about 17% due to the existence of the trailing vortex. These rough estimations suggest that the additional resistance caused by the existence of the vorticity on the line vortex will be about 10% after cancelling each other.

However, in our computation, all the simulations are performed without taking the trailing vortex and the vertical velocities into consideration. This approximation makes the computation much simpler otherwise the difficulty may happen how to determine the trailing vortex lines which may touch the hull when the line vortex is placed at forepart.

Eventually, the induced velocities by a pair of line vortices are computed and used as a base flow for the Rankine source method, in which the total velocity potential can be obtained to satisfy the full boundary conditions as following sequence of steps;

- Calculation of the induced velocity by the line vortex at the hull and free surface panels.

- Hess and Smith method calculation including the induced velocity on the hull surface due to the line vortex.

- Wavy velocity potential calculation based on the basic flow of the induced velocity on the free surface due to the line vortex.

- Final ϕ_o and ϕ_w will be obtained iteratively as same procedure with the aforementioned Rankine source scheme.

3.2 Pilot computation

We carry out some pilot computations at first for the Series 60 with and without wings in order to verify the present computational scheme. The wings are flat plate and attached to hull. They are assumed to have a span of 50% ship breadth($B/2$) and a chord of 2.5% ship length($L/40$). The depth of the wing is a half of the design draft

of the ship. The location of the wings is at 5% aft from F.P. and the angle of attack is -5 degrees to produce a downward lifting force. The lifting force by the wings is about 1.7% of the ship displacement. In the computation, wing is replaced by a circulation distribution over a line vortex which produces a comparable lifting force to the wing mentioned above.

Fig.(3.5) illustrates the computed and measured wave profiles for the Series 60 with and without wings at the speed of the Froude number 0.31. The measurements are carried out at the towing tank. The computed results show good agreements with the measured except the bow region which is common in other computations by the Rankine source method. To be encouraging, the effects of the wings are prominent even in the results of calculations as well as those of measurements. Furthermore, their quantitative differences are also fairly coincident. We can conclude that the present numerical scheme is proved to be very effective on the simulation of wing system although the wing is approximated by a lifting line neglecting the contribution of the trailing vortex.

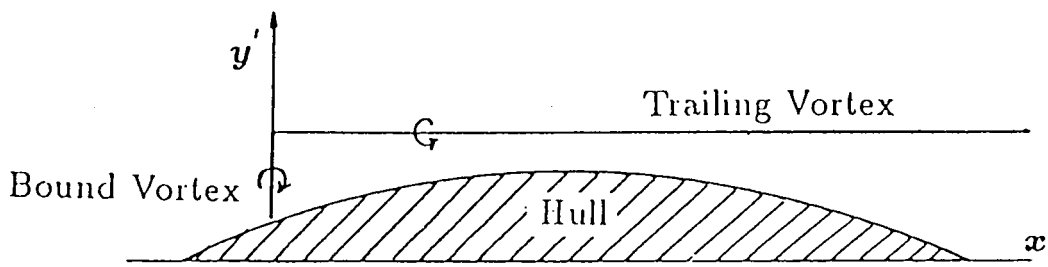

Fig.(3.1) Shape of line vortex

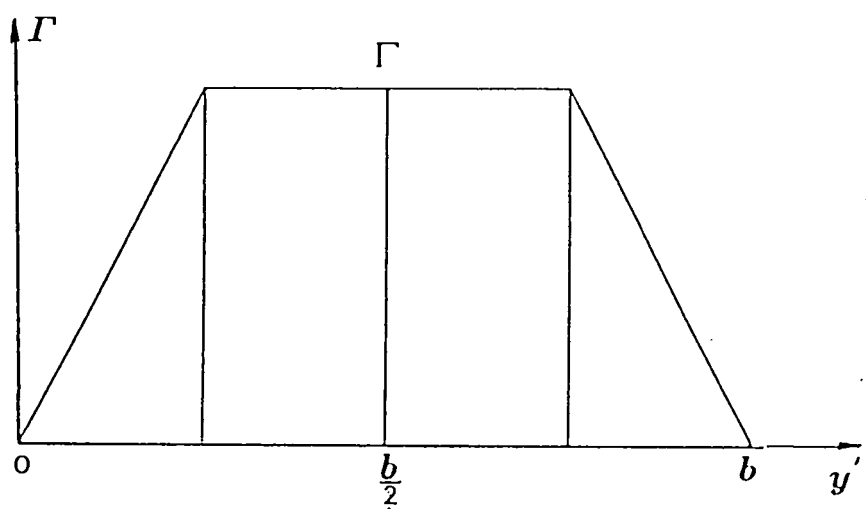

Fig.(3.2) Circulation distribution

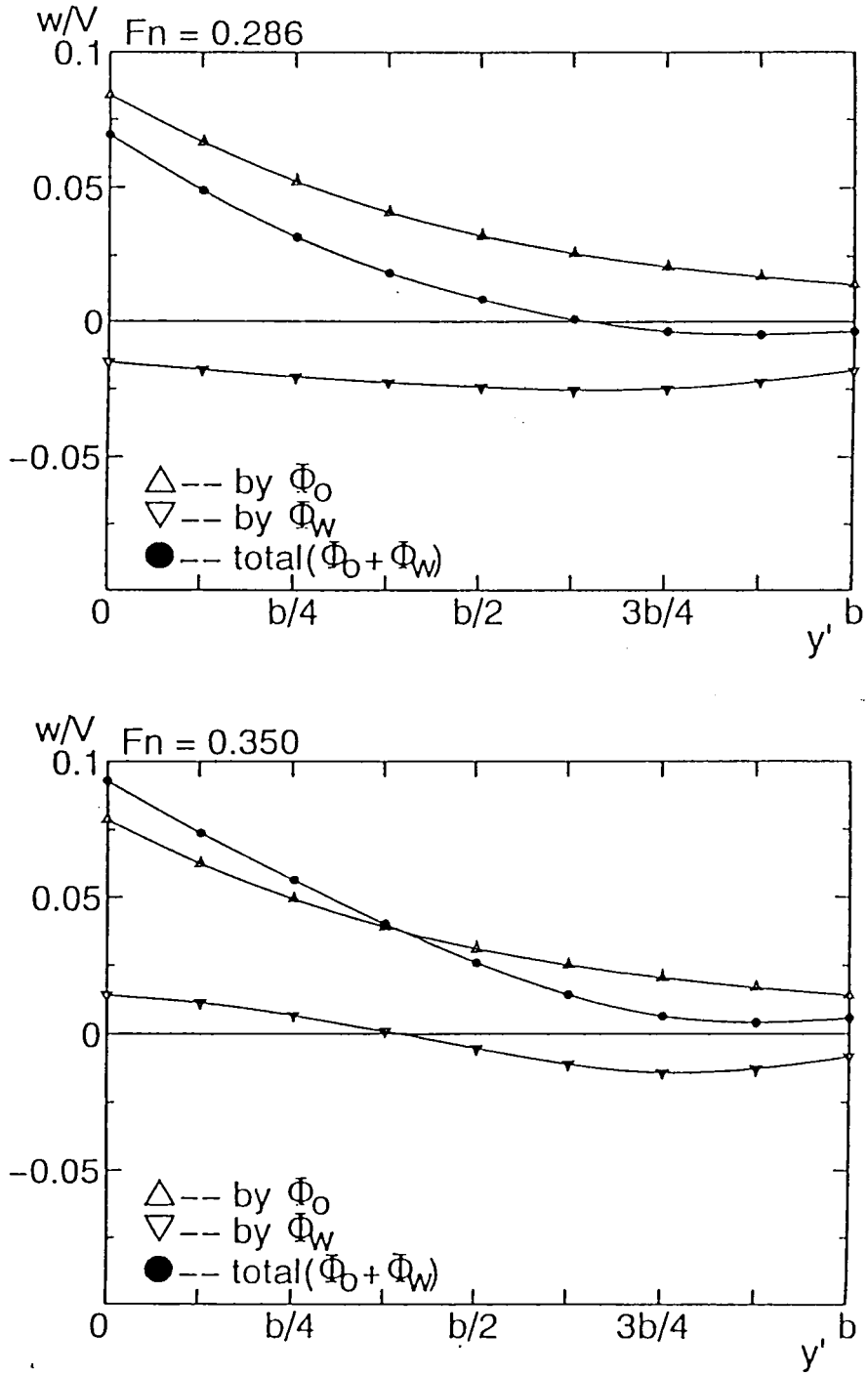

Fig.(3.3) Computed vertical velocity components on line vortex

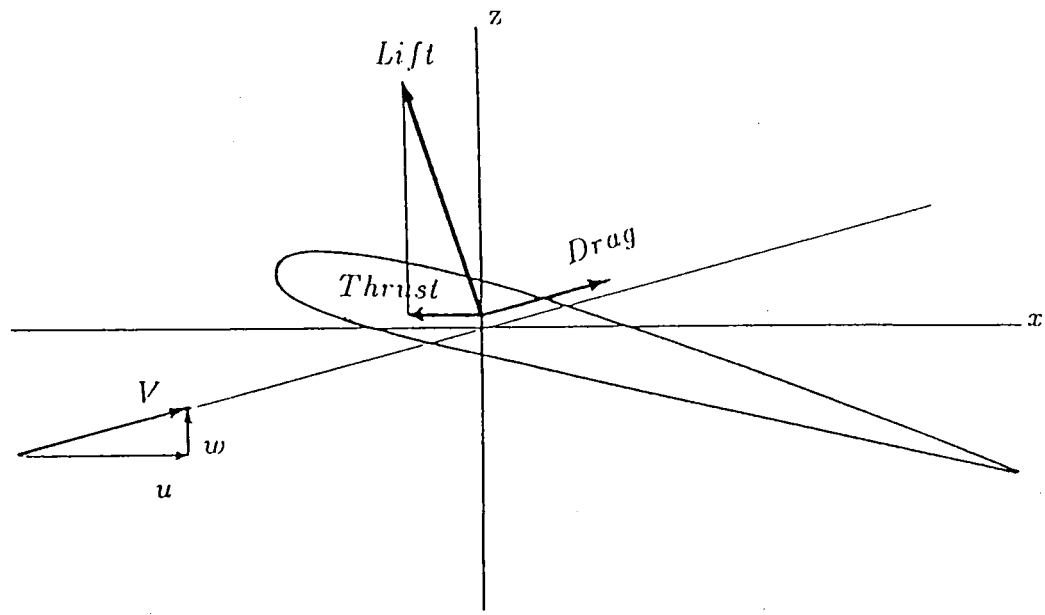

Fig.(3.4) Force components

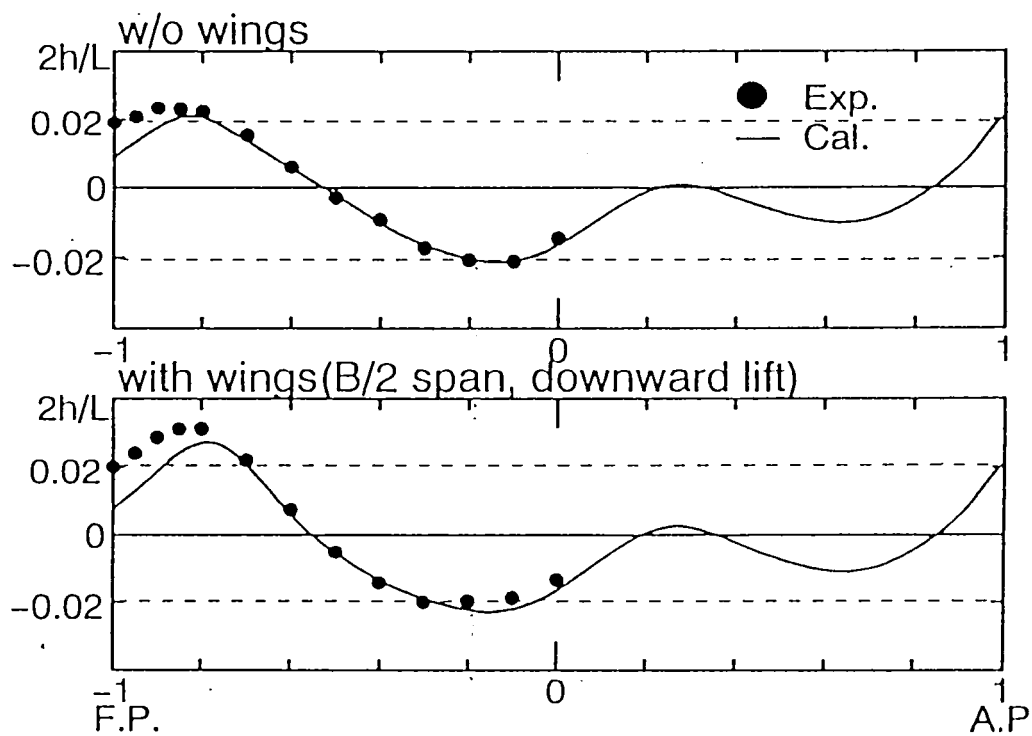

Fig.(3.5) Comparison of wave profiles of Series 60 with and without wings(Fn=0.31)

4 Simulation on Wave Reduction by Wings

4.1 Vortex strength

Based on the verification by the pilot computation, we study the effects of the vortex strength and location on the wave resistances and wave patterns for the Series 60. The span of the flat plate wing is 25% ship breadth(B/4) and the angle of attack is fixed to be ±5 degrees.

Fig.(4.1) and Fig.(4.2) show the hull side wave profiles and the pressure contours on the hull for the different strengths of the line vortex lying at x=-0.9; the Froude number is 0.35. The lifting force indicated there is the ratio to the buoyancy force which is modified by changing the chord length. In the downward lift case indicated by -2.2% lift in Fig.(4.1), the velocity near the free surface is decelerated and consequently generates high pressure region locally. This high pressure makes the wave arise; a big wave peak just behind the location of the line vortex can be observed. On the contrary, the upward lift accelerates the velocity and lessens the pressure near the free surface. This compels the wave height down. With the increment of the upward lift strength, the original wave height becomes gradually small. It is esteemed that this flow mechanism may reduce the ship wave pattern resistance. As later shown in Fig.(4.7), the reduction of wave resistance can be 30%. Fig.(4.3) shows the corresponding wave patterns. As clearly seen, the wave crest is gradually decreasing with the increment of the strength of the upward lifting force. The wave height is much increased in case of the downward lifting force.

Masuko et al.[4] have carried out some model tests to reduce wave breaking phenomena by installation of a wing just in front of the stem of a conventional ship where about 10% reduction of the residual resistance of the ship were seen over operating speed ranges. He explains that the wing accelerates the flow velocity to lessen the high pressure near the bow and finally prevents the severe wave breaking. The present computational simulations show the same mechanism of flow acceleration and have same tendency as their experimental results.

Fig.(4.4) shows the computed wave making resistance where the span of the line vortex is B/2 and the vortex is placed at x=-0.9. The angle of attack is fixed, so that the lifting forces are varying in accordance with the Froude number. Two angles of attack are selected to generate an upward lift and also a downward lift. The amount

of the wave resistance reduction by the upward lift is reaching well over 20% for all the Froude numbers. On the contrary, the wave resistance with the downward lift is much increased. The result shows that the reduction of the wave resistance by the wings is quite persistent even in a wide range of speeds as observed by Masuko[4].

4.2 Vortex location

The calculations of wave profile and resistance are carried out for various locations of the vortex at two Froude numbers. This is because the vortex locations and their effects are also important in order to find the best position of the wing in view of wave resistance. Fig.(4.5) presents the results for the three different locations of the vortex; x=0.9, 0.0 and 0.9. The vortex produces 2.2% upward lift at the Froude number 0.35. By the existence of the line vortex at a certain location, the wave generated by hull is locally interacted to make the resistance reduced or increased. Fig.(4.6) shows the comparison of the wave patterns at different locations of the vortex. The wing located at x=-0.9 seems most effectively cancelling the wave.

Fig.(4.7) shows the variation of wave resistances; the ratio is defined as $C_w\ ratio = \{C_w(vortex) - C_w(w/o)\}/C_w(w/o)$ where $C_w(w/o)$ is the resistance without wings. From these results, we can easily know that the vortex generating the upward lift cancels the original wave peak and lessens the wave resistance if the vortex is located at the starting part of the wave crest where the w component is positively maximum. Especially at the stem, where a bulb is normally placed, is the best place to reduce the wave resistance. The results show also that the effective place of the wing depends on the Froude numbers as naturally accepted. It is important to select a proper location at each Froude number.

4.3 Multiple vortices

We investigate a case of the hull with two pairs of wings. The wings are also replaced by line vortices. Vortices are located at x=-0.9 and +0.95, where the wave resistance reductions are expected to be very large from the computation results of Fig.(4.7). Fig.(4.8) shows the wave profile and patterns for the two pairs of line vortices with the same circulation strengths at both the locations and Fig.(4.9) with the twice strength at x=0.95 but same at -0.9. From the computation results, we can find 70% $\sim$ 80% of the original wave resistance can be reduced with these two pairs of line vortices.

Although the computation is based on the assumption of the potential flow and the viscosity of the fluid is ignored, a possibility for the large reduction of the wave resistance by the installation of stern wings is expected especially for the case of the ship generating a big stern wave. Considering the aforementioned simulation result of the Series 60 showing a good agreement with the measured result even in the stern wave profile, the idea to reduce the wave resistance by the stern wings is probably very effective and very realistic.

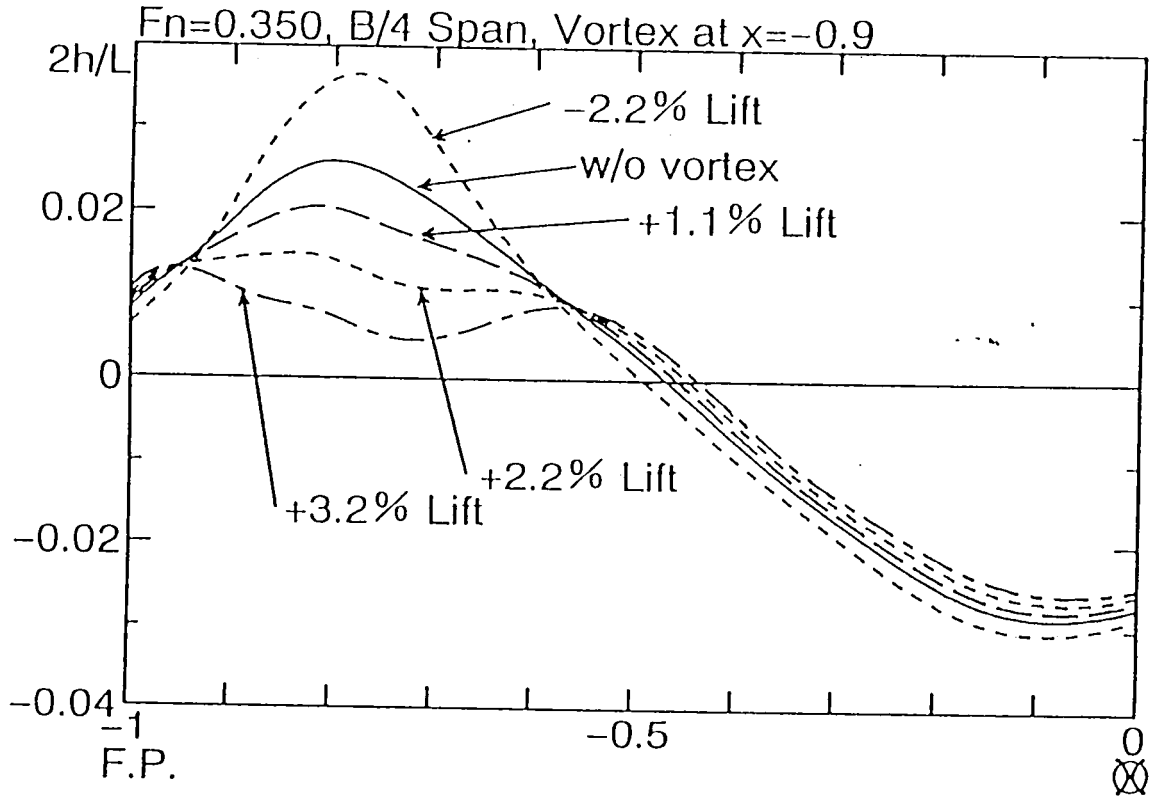

Fig.(4.1) Comparison of the variation of wave profiles due to vortex strength

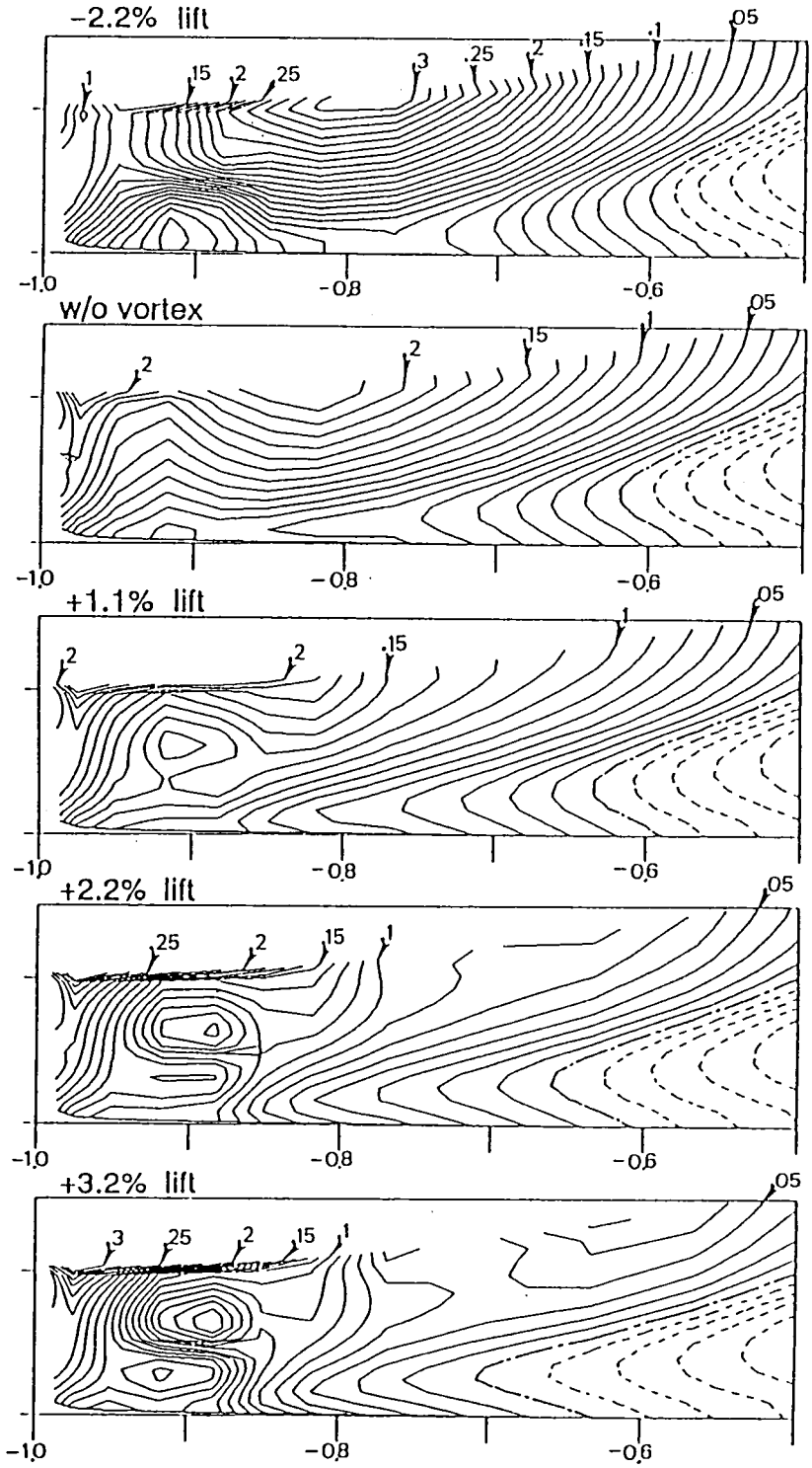

Fig.(4.2) Comparison of the variation of pressure contours due to vortex strength(Fn=0.35)

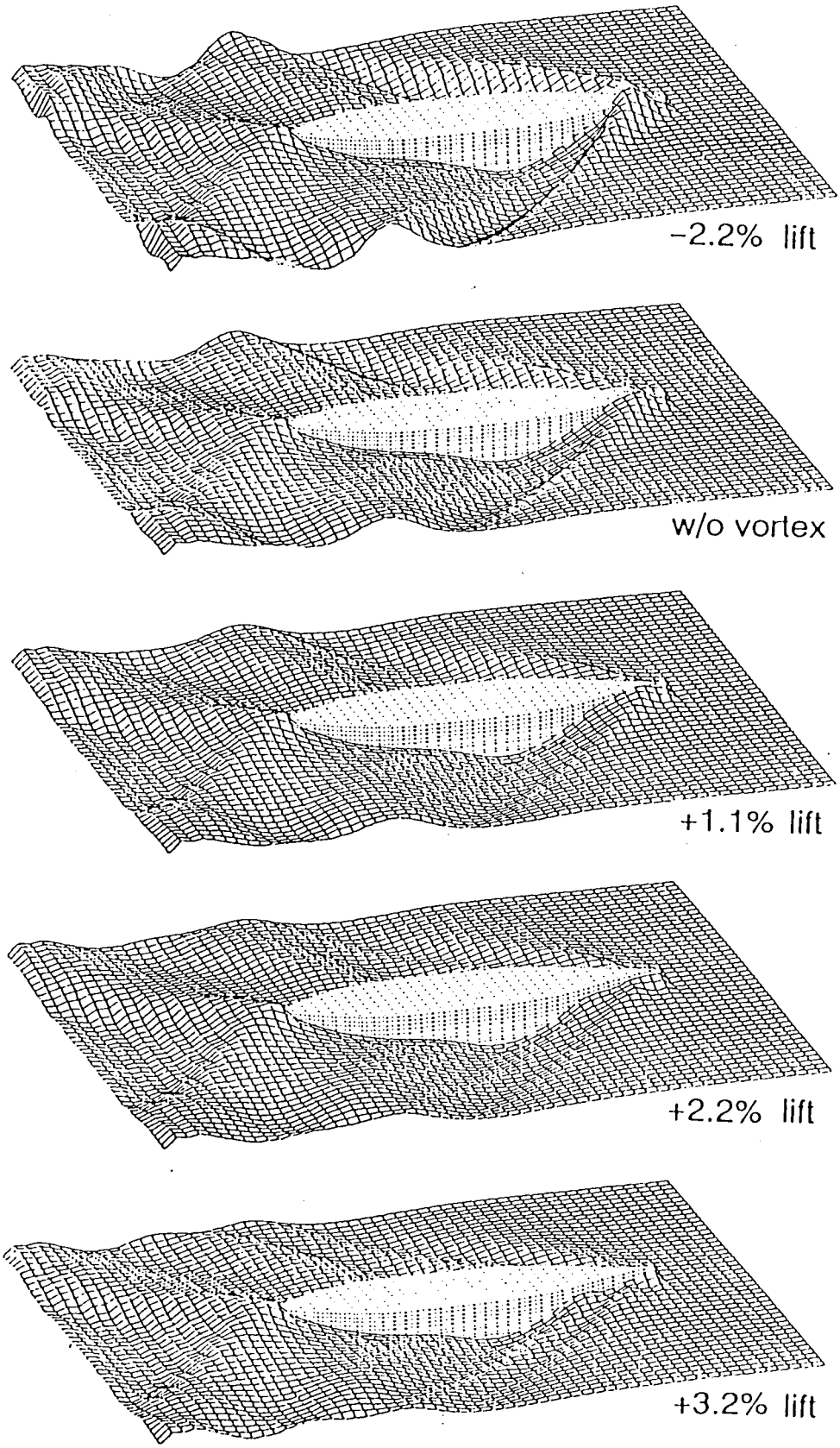

Fig.(4.3) Comparison of the variation of wave patterns due to vortex strength(Fn=0.35)

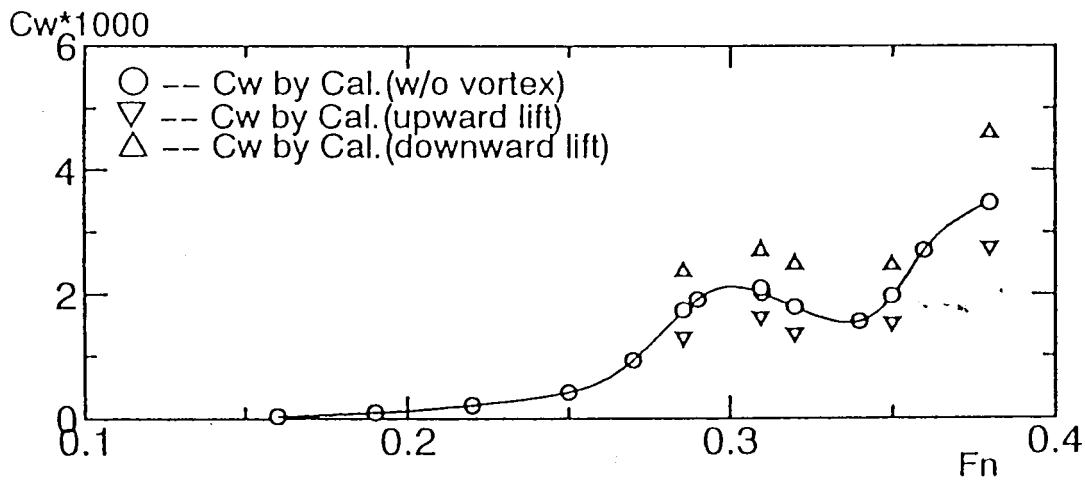

Fig.(4.4) Comparison of computed wave resistances of Series 60 with and without wings (x=-0.9)

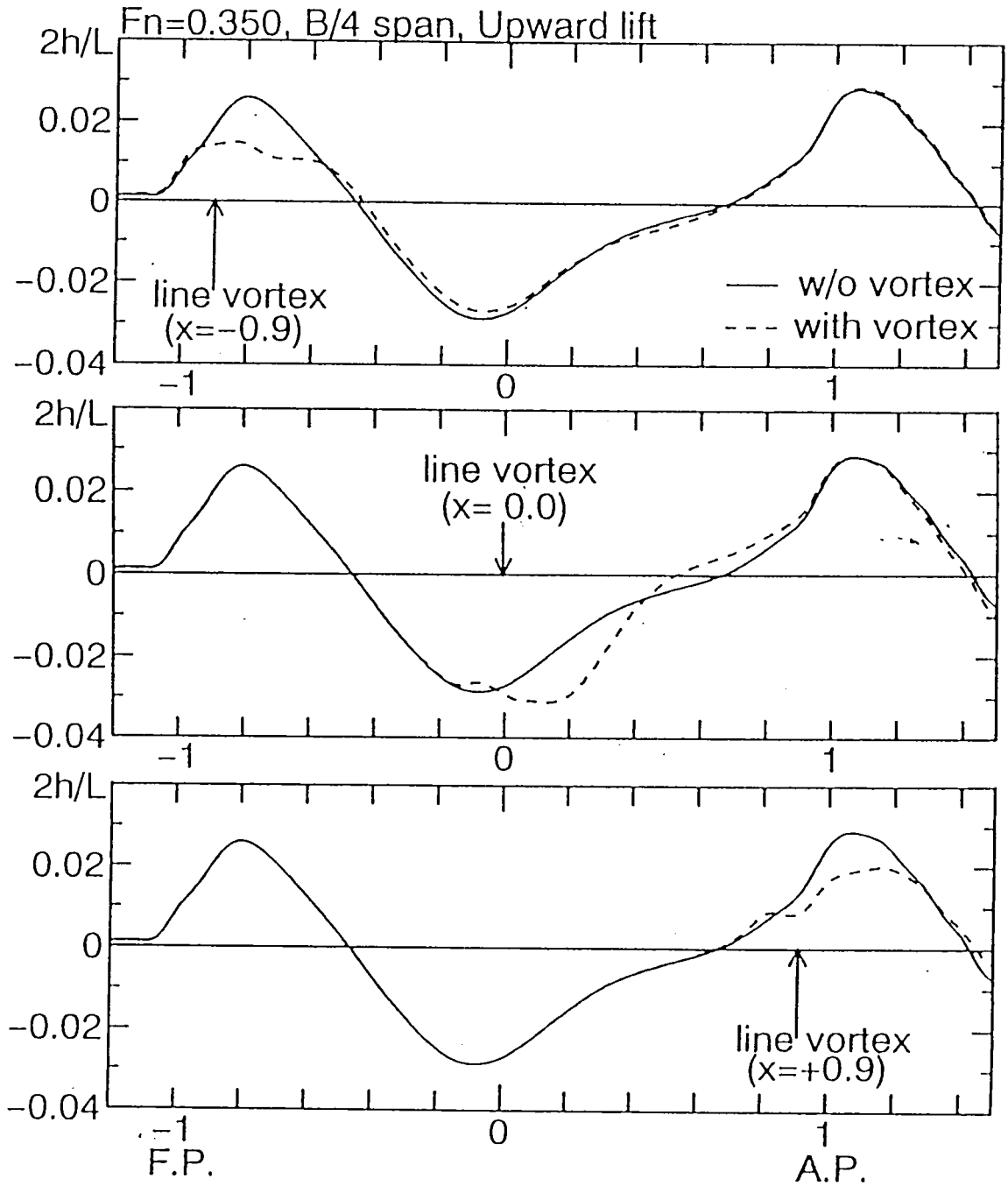

Fig.(4.5) Comparison of the variation of wave profiles due to vortex location(Fn=0.35)

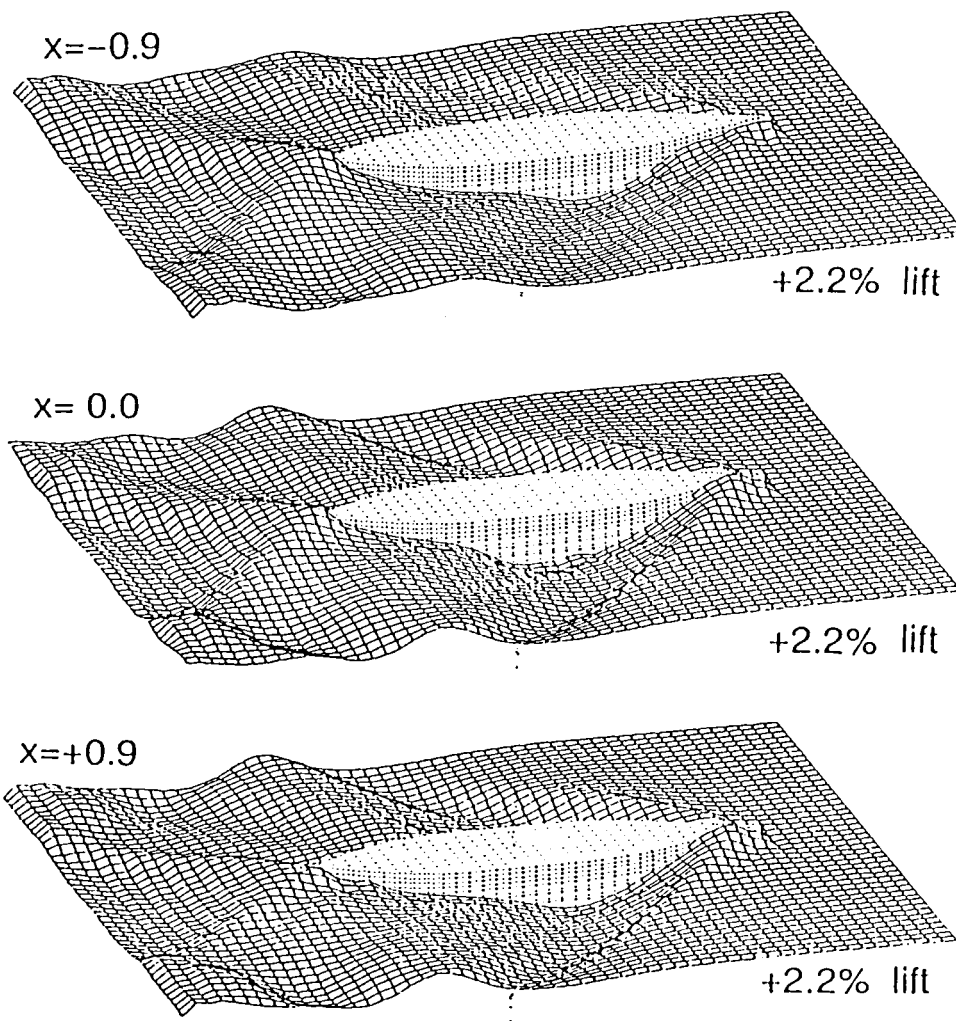

Fig.(4.6) Comparison of the variation of wave patterns due to vortex location(F_n=0.35)

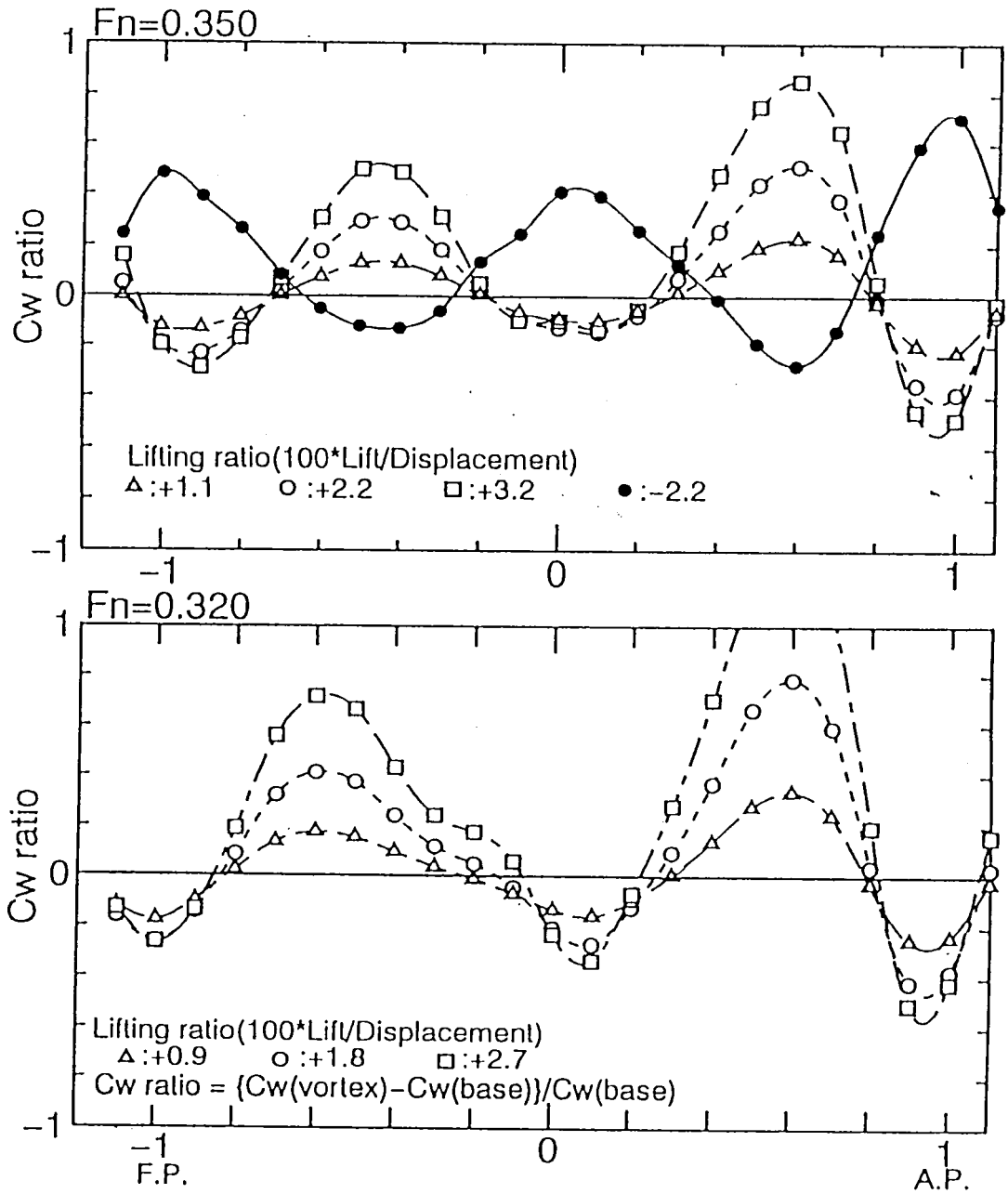

Fig.(4.7) Comparison of wave resistances due to vortex location and strength

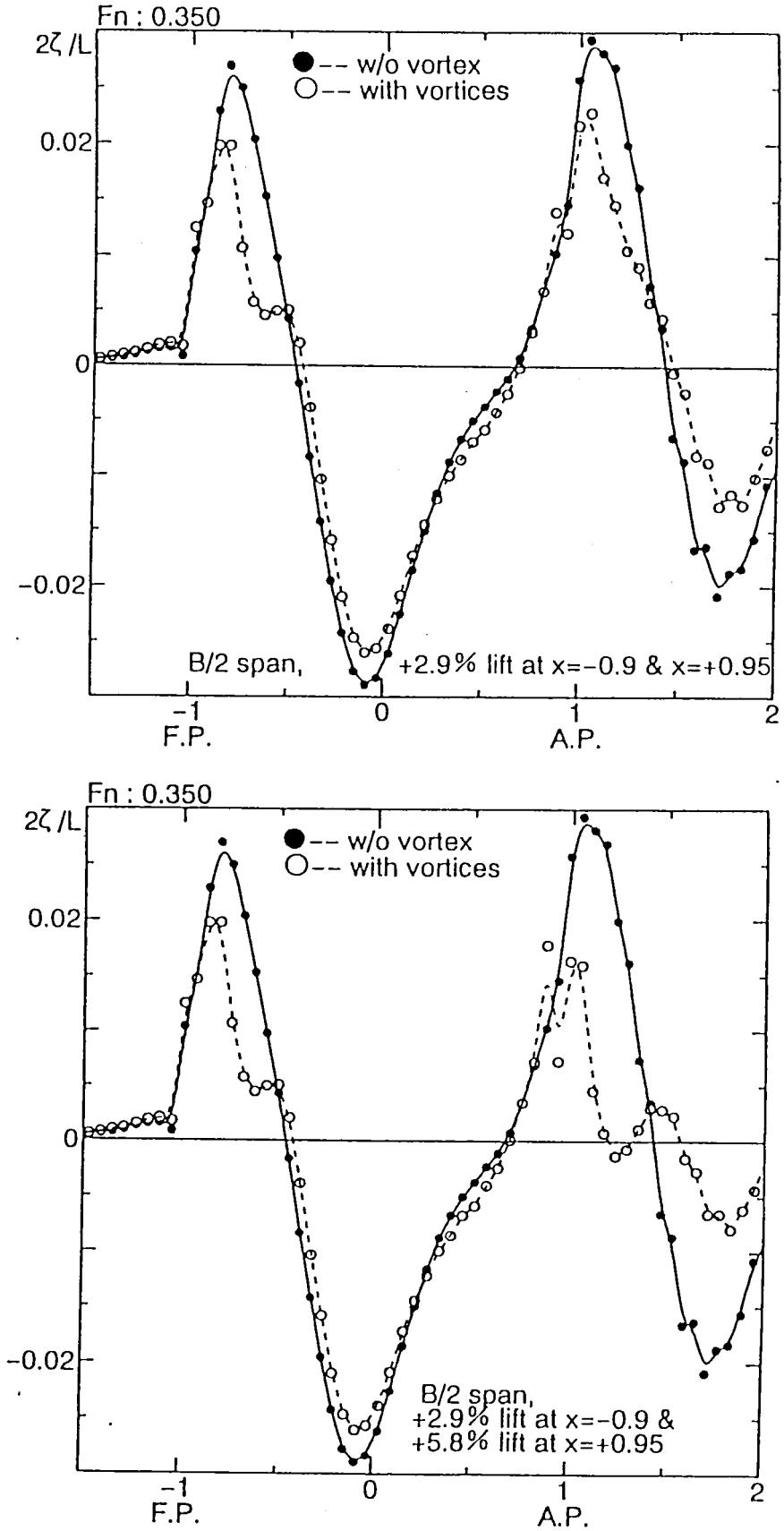

Fig.(4.8) Comparison of computed wave profiles of two pairs of line vortices

+2.9% lift at x=-0.9 & x=+0.95

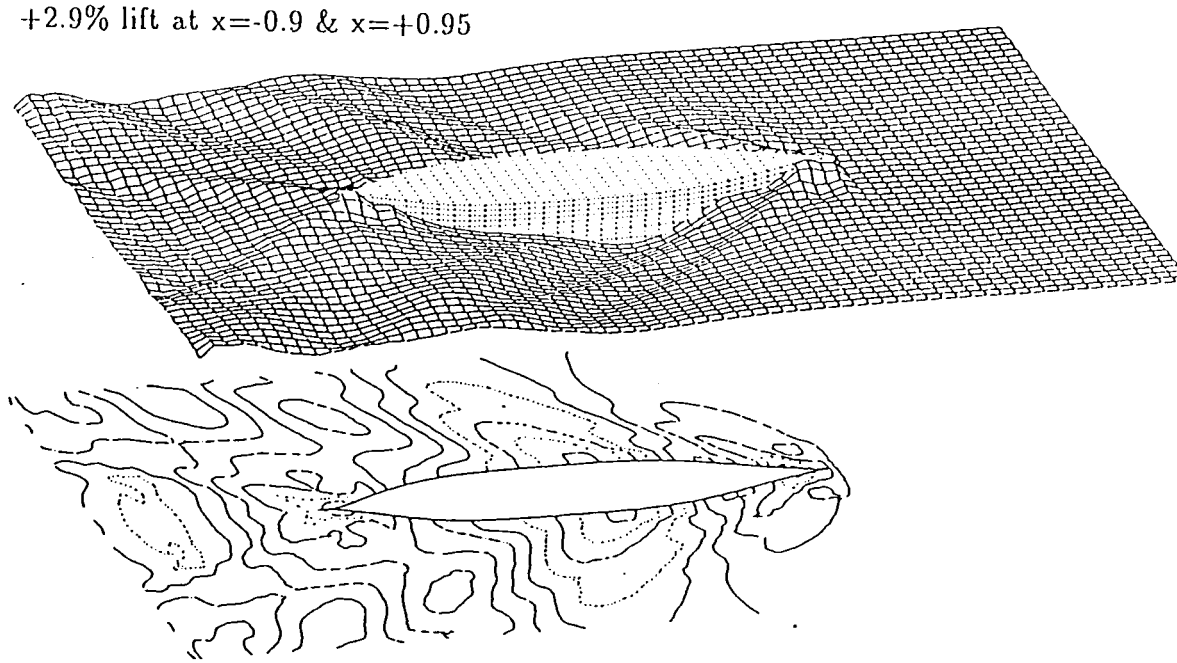

+2.9% lift at x=-0.9 & +5.8% lift at x=+0.95

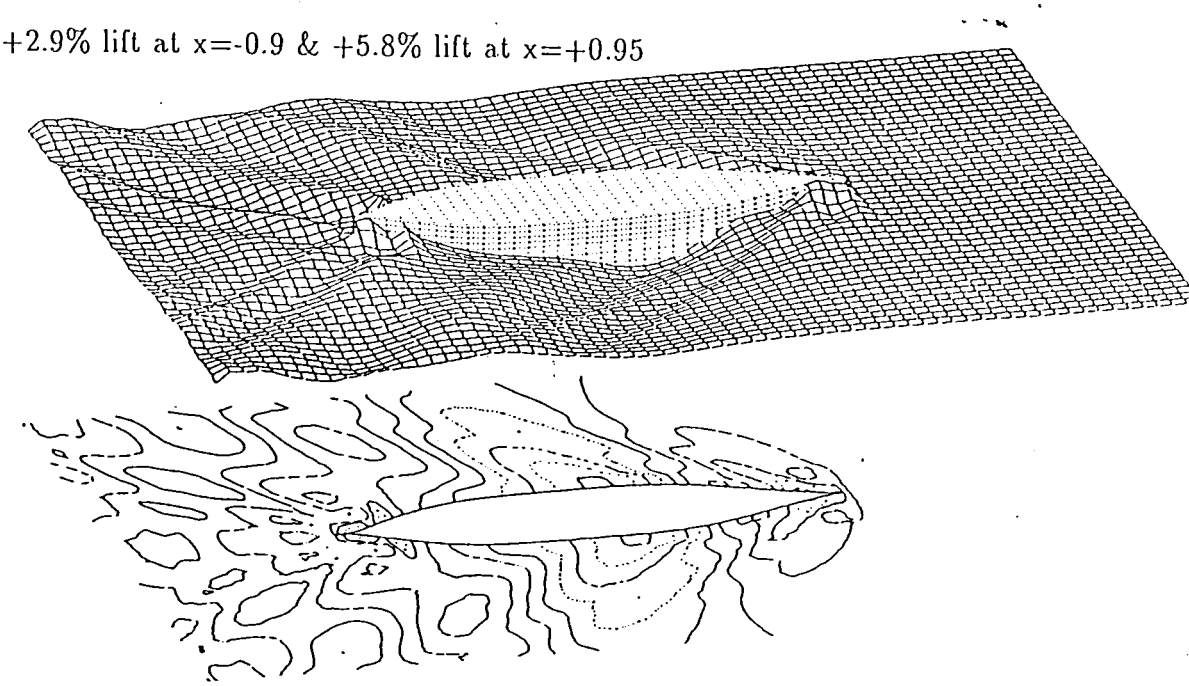

Fig.(4.9) Comparison of computed wave patterns of two pairs of line vortices

5 Confirmation by Experiments

In order to confirm the above results by simulation, the wave profiles were measured at four Froude numbers of 0.29,0.32,0.35 and 0.38. The principal dimensions for the tested Series 60 model and wings are presented in Table (5.1). The wings are attached to the hull as seen in Fig.(5.1) to generate upward and downward lifting forces by changing their angle of attack. The section shape of the wing is flat plate but with slight modification as shown in Fig.(5.1). Measurements are carried out at towing tank with the model fixed.

Table.(5.1) Principal dimensions of ship model and wing

ship model particulars	
Length between perpendiculars	1.800 m
Breadth	0.240 m
draft	0.096 m
Block coefficient	0.600
wing particulars	
Span	0.120 m
Chord	0.045 m
Angle of attack	$\pm 5 deg.$
Location in x-dir.	0.090 m from F.P.
in z-dir.	0.048 m above B.L.

Fig.(5.2) $\sim$ (5.5) show the comparison of the computed and measured wave profiles along the hull side at four different Froude numbers. Both the computed and measured results show exactly the same tendencies; the downward lift increases the wave and the upward decreases. It can be also mentioned that even the quantitative differences are well predicted by the present computations where the wings are simulated only by a pair of vortices.

A noticeable difference between the computed and the measured can be found in the case of the wings generating upward lift; a strong wave fluctuation behind the wing can be seen in the experiments but not so much in the computations. These may be caused by the following reasons. The flow around the bow is passing obliquely from the lower parts of the bow to the upper parts, which was already proved by the investigation of the vertical velocity components on line vortex as shown in Figs.(3.3) and (3.4). The average vertical velocity component at Fn=0.35 is esteemed to be about

1.4% compared with the uniform flow. This non-horizontal flow makes angle of attack larger than the geometrical angle of 5 deg. and consequently more strong circulation than that of the calculation may be produced. To confirm the above, we carry out one more computation for the upward lift case with the slightly stronger circulation at Fn=0.286. As shown in Fig.(5.6), the simulation result is improved with this modification.

We can conclude that the present simulated results are well confirmed through the experiments for the wide range of the Froude numbers. The discrepancy between the computation and the experiment can be improved much by more precise control of the angle of attack and by the consideration of more realistic circulation distribution along the wing even if the lifting line theorem is used.

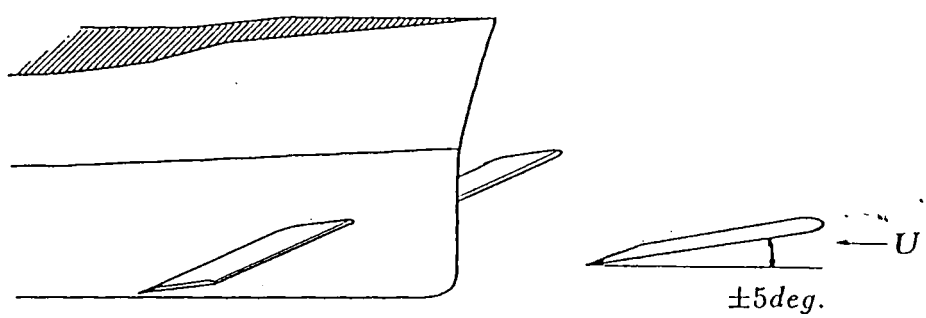

Fig.(5.1)Sketch of wing system and wing section for model test

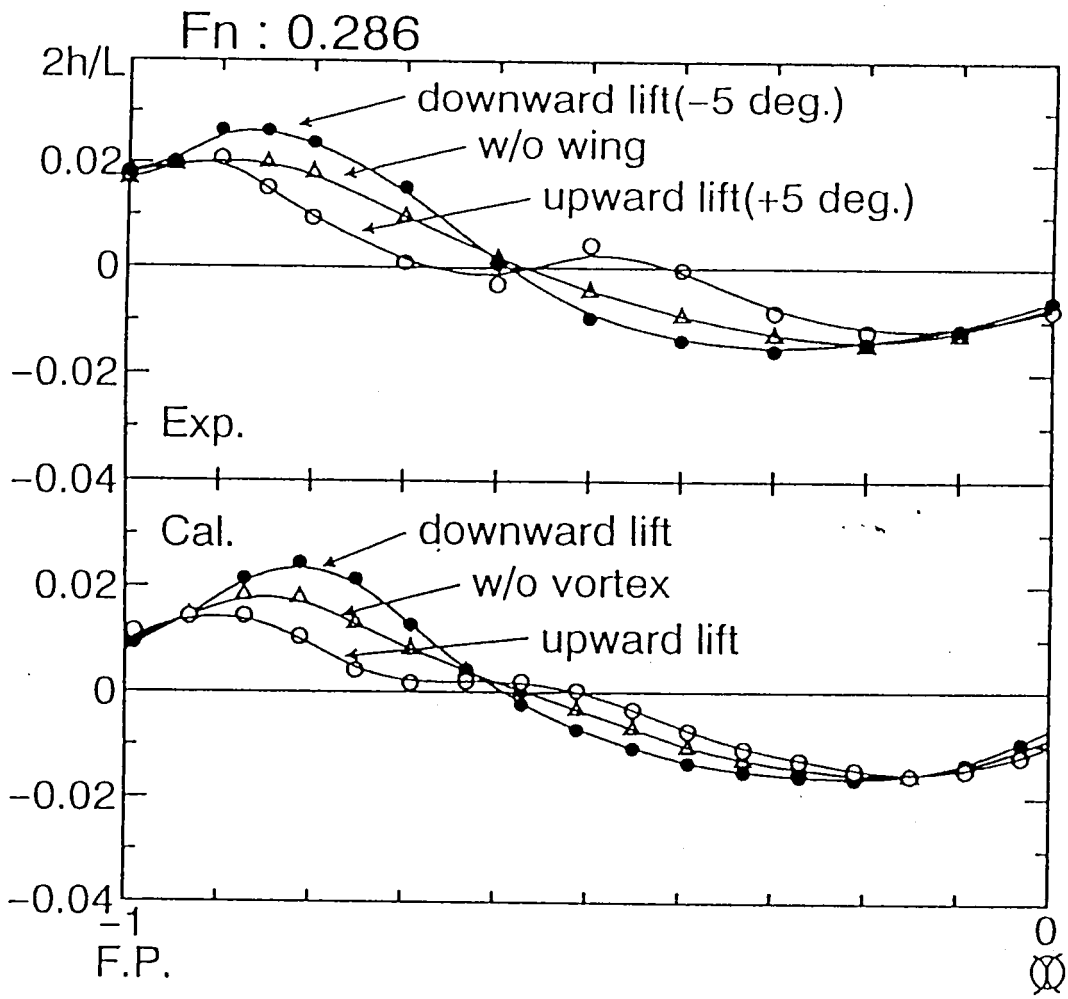

Fig.(5.2) Comparison of computed and measured wave profiles of Series 60 with wings (Fn=0.286)

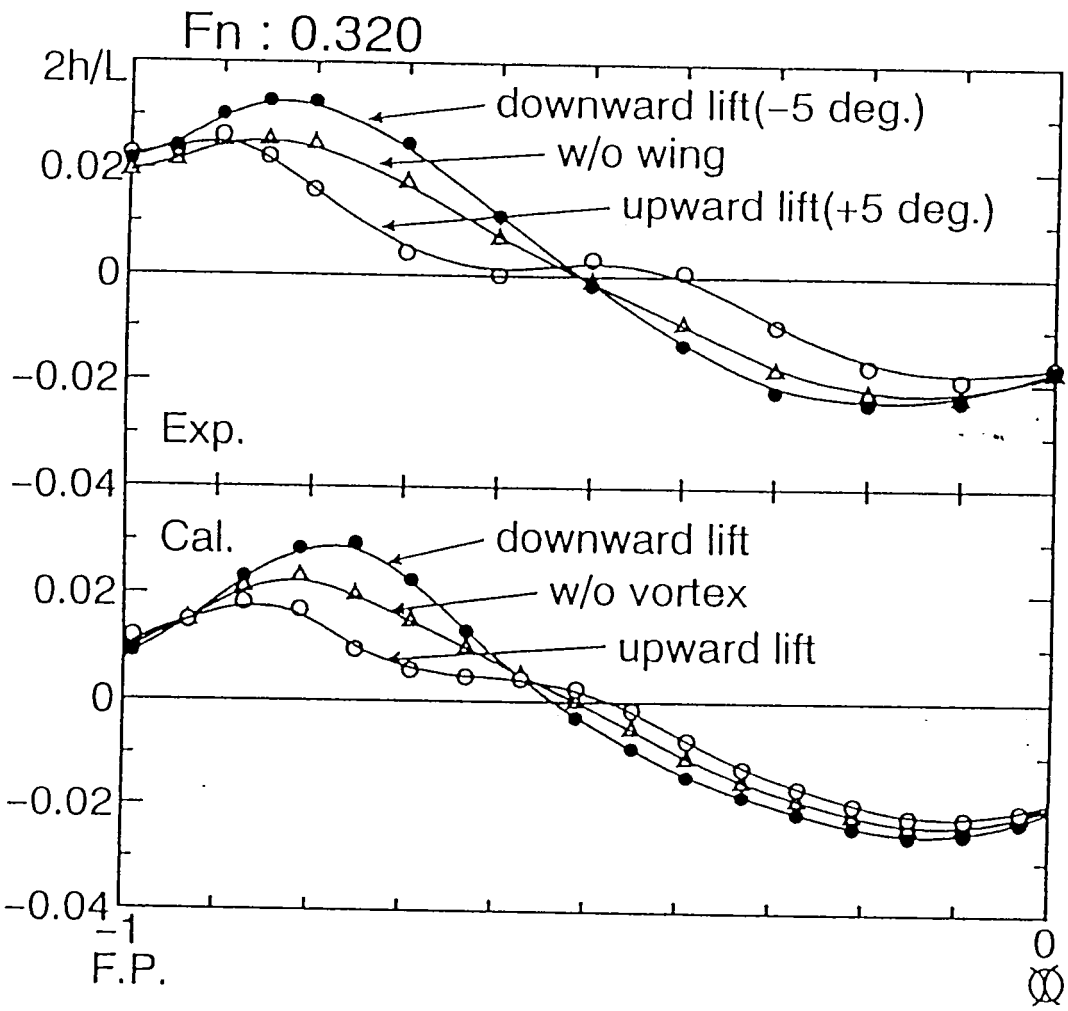

Fig.(5.3) Comparison of computed and measured wave profiles of Series 60 with wings (Fn=0.320)

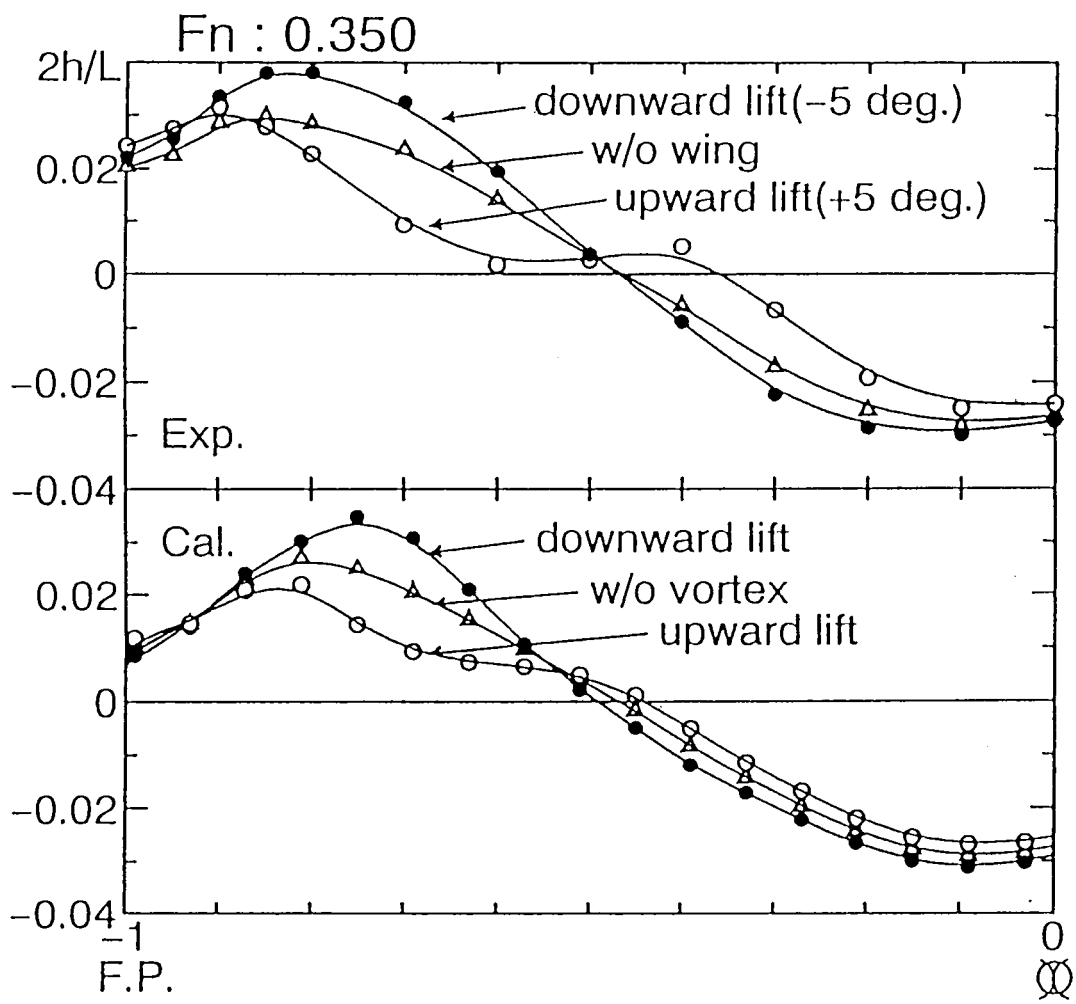

Fig.(5.4) Comparison of computed and measured wave profiles of Series 60 with wings (Fn=0.350)

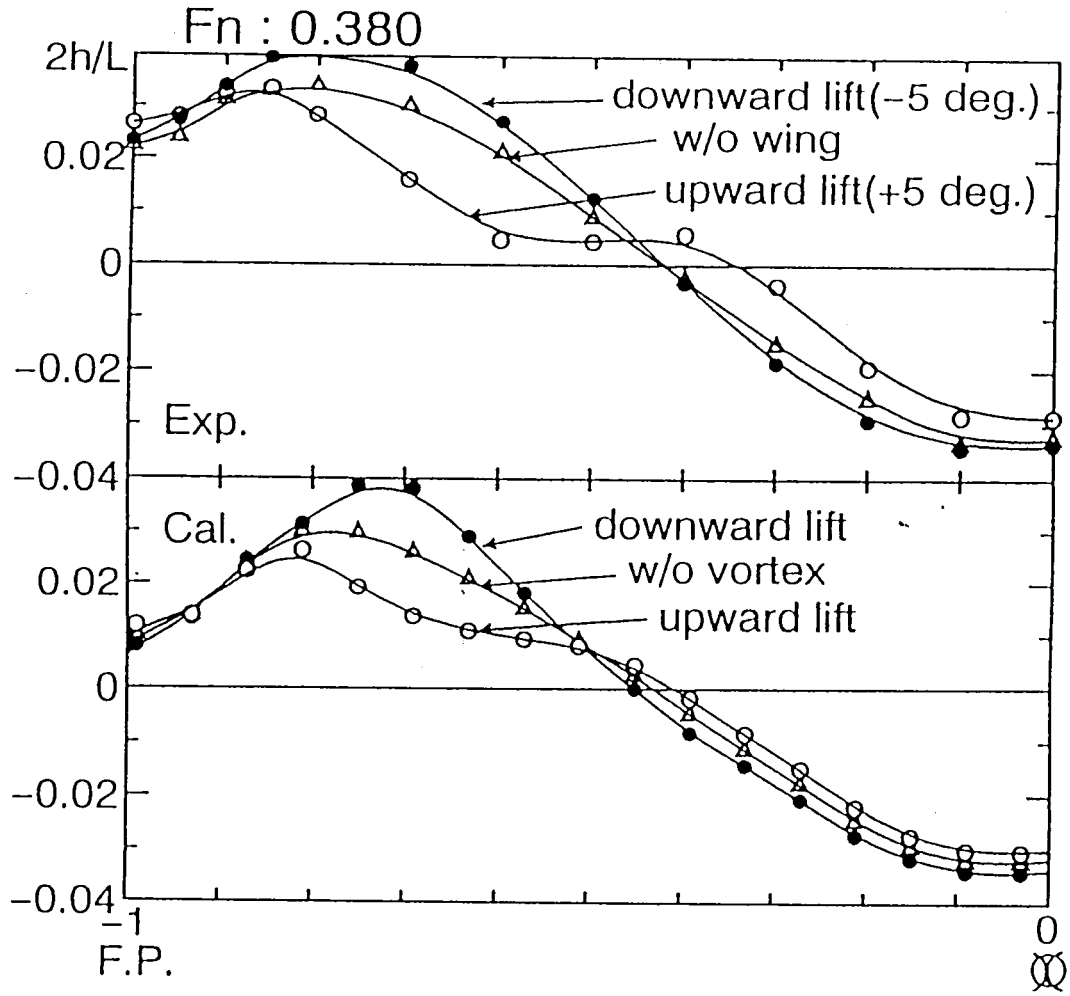

Fig.(5.5) Comparison of computed and measured wave profiles of Series 60 with wings (Fn=0.380)

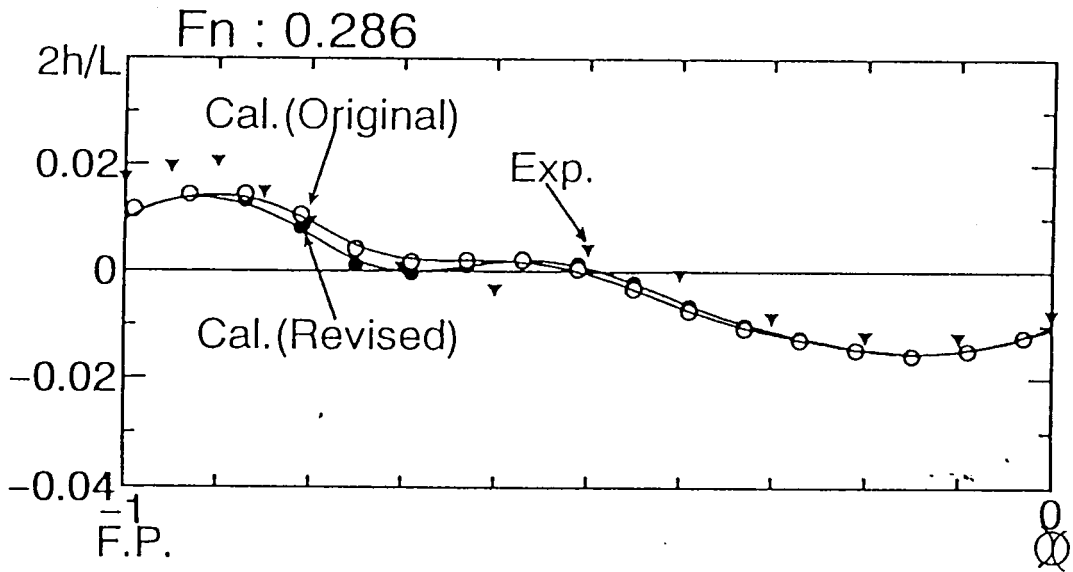

Fig.(5.6) Comparison of computed and measured wave profiles for a revised circulation(Fn=0.286)

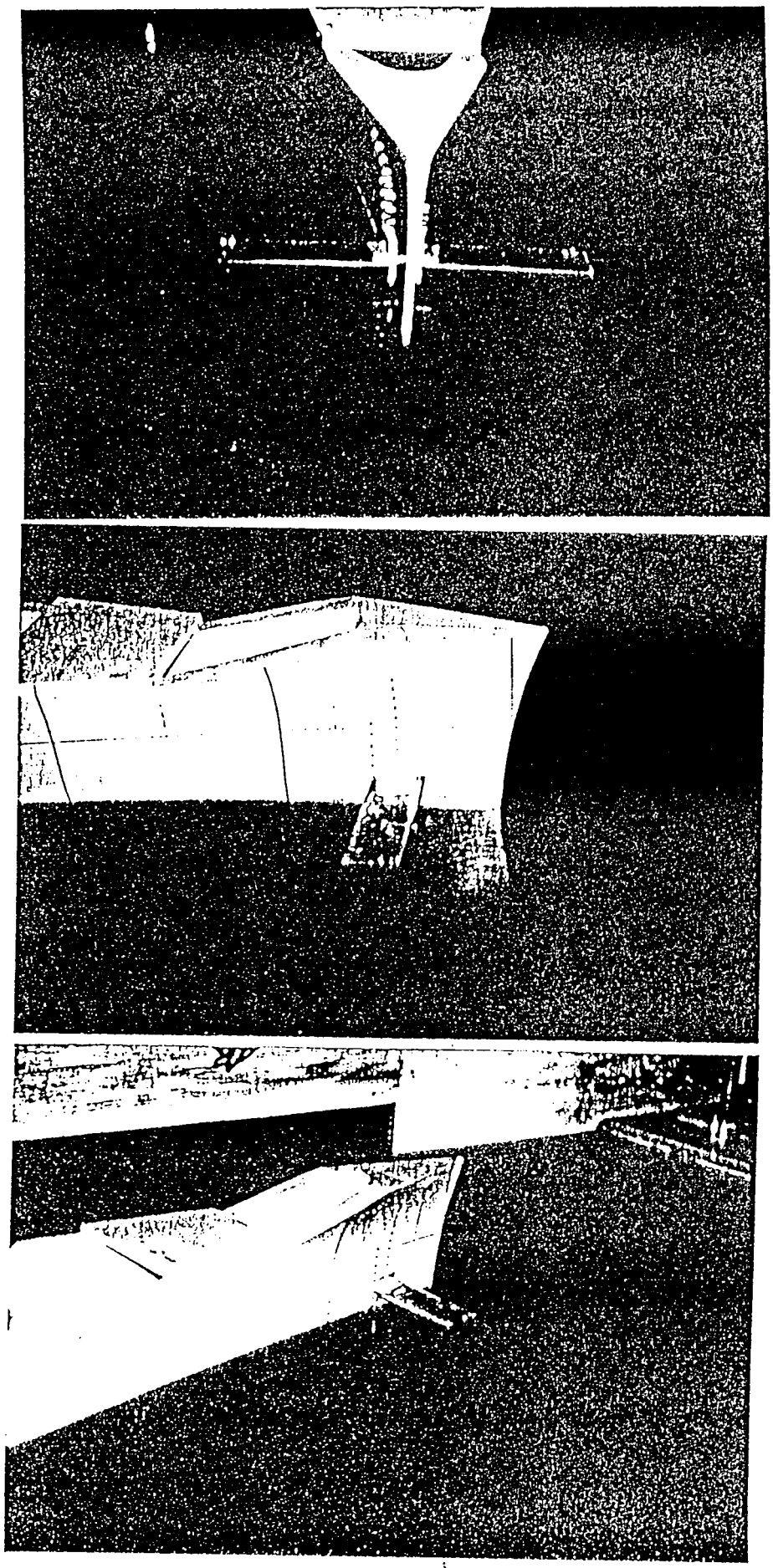

Poto.(5.1) Series 60 with a pair of wings

6 Concluding Remarks

A modified Rankine source scheme is suggested and investigated its usefulness for the various hull forms. The double model flow velocity potential is modified to contain the effect from the wavy velocity potential and total velocity potential is obtained with the iterative procedure to satisfy both the hull and free surface boundary conditions. As a further application of the method, the flow and resistance are simulated for the ship with wings where the wings are assumed as a pair of lifting lines. Findings are summarized as follows.

1) The Rankine source method modified from Dawson's original shows the quite acceptable results for the various simulations of three diverse hull forms including an actual full ship.

2) The present computation method based on the lifting line approximation well corresponds to the experimental results of the hull with wings.

3) The wave height can be decreased by a wing which is producing an upward lift. This is because the velocities behind the wing are accelerated by the circulations and the high pressure is reduced. Conversely the downward lift increases the wave elevation.

4) The best position of the wing for the reduction of the wave resistance is near the stem or stern of the ship because the wave crest by the bow or stern wave are normally locating there and the wave cancellation can be expected effectively by an interaction between the hull and wings with upward lift.

5) The amount of the reduction by the wings with a constant angle of attack is persistent even for the wide range of speeds.

6) It may be possible to reduce the wave resistance more effectively if wings generating proper lifting force are installed on the hull and furthermore multiple wings are properly considered.

7 References

[1] Ando, J., Kataoka, K., Nakatake, K.: *Rankine Source Method in High Speed Range, The West-Japan Soc. of Nav. Arch. Japan. No.84, (1992), pp.1-10.*

[2] Dawson, C. W.: *A Practical Computer Method for Solving Ship-Wave Problems, Proc. of 2nd Intern. Conf. on Numerical Ship Hydrodynamics, Berkely, (1977), pp.30-38.*

[3] Ikehata, M.,Suzuki, K., Hosoi, H., Tahara, Y.: *Availability Study of Rankine Source Method to Computation of Waves and Wave-making Resistance of High Speed Ships, Workshop on Wave Resistance and Viscous Flow, University of Tokyo, (1994), pp.3-23.*

[4] Masuko, A., Ogiwara, S.: *A study on the Wave Breaking Phenomena around Ship Hull, IIII Technical Report, Vol.25, No.5, (1985), pp.280-285.*

[5] Mori, K., Nishimoto H.: *Prediction of Flow Fields around Ships by Modified Rankine Source Method, JSRA, Japan, Vol. 150, (1981)*

[6] Mori, K.: *Comments on Papers Presented at the Workshop on Wave Resistance, JTTC Report No. 1980-I-1, (1980)*

[7] Nakatake, K., Kawagoe, T., Kataoka, K., Ando, J.: *Calculation of the Hydrodynamic Forces Acting on a Hydrofoil, The West-Japan Soc. of Nav. Arch. Japan. No.76, (1988), pp.1-13.*

[8] Nakos, D.E., Sclavounos P.D.: *On Steady and Unsteady Ship Wave Patterns, J.Fluid Mech., Vol 215, (1990), pp.263-288.*

[9] Nakos, D.E., Sclavounos P.D.: *Ship Motions by a Three-Dimensional Rankine Panel Method, 18th Symposium on Naval Hydrodynamics, Ann Arbor, Michigan, (1990). pp.21-39.*

[10] *Proceedings of CFD Workshop Tokyo 1994, SRI, Tokyo, (1994).*

[11] Yasukawa, H.: *Calculation of Free-Surface Flow around a Ship in Shallow Water by Rankine Source Method, 5th Inter. Confer. on Numerical Ship Hydrodynamics, Hiroshima, Japan, (1989), pp.451-461.*

[12] Minle-Thomson, L.M.: *Theoretical Hydrodynamics, Fifth Edition, The Macmillan Press, (1968), pp.55.*

Appendix Formula of Wave Resistance

The force acting on a body, F is given by

$$F = -\int\int_{S_H} npdS \tag{A.1}$$

where n : normal vector, p : pressure and S_H : body surface. If the flow is inviscid Eq.(A.1) can be written in another form;

$$F = -\rho\int\int_{S_H} wdS \tag{A.2}$$

where ρ : density and

$$w = n\frac{p}{\rho} + q(n\cdot q) = -\frac{1}{2}nq^2 + q(n\cdot q) \tag{A.3}$$

where q : velocity. The second term of rhs of Eq.(A.3) is always zero on S_H due to the body surface condition. Applying the Gauss theorem[10] to the fluid domain V, we have

$$\begin{aligned}&\int\int_{S_H} wdS + \sum_i \int\int_{S_i} wdS + \int\int_{S_\infty} wdS \\ &= \int\int\int_V \{\frac{1}{2}\nabla q^2 - q(\nabla\cdot q) - (q\cdot\nabla)q\}dV\end{aligned} \tag{A.4}$$

where S_i is a small semi-sphere surrounding a singularity and S_∞ is the surrounding surface of V as seen in Fig.(A.1).
In Eq.(A.4),

$$\frac{1}{2}\nabla q^2 - (q\cdot\nabla)q = q\times(\nabla\times q) = q\times\omega \tag{A.5}$$

$$q(\nabla\cdot q) = 0$$

where ω is the vorticity defined by $\omega = \nabla\times q$.
Then, we have

$$F = \rho\sum_i \int\int_{S_i} wdS + \rho\int\int_{S_\infty} wdS - \rho\int\int\int_V (q\times\omega)dV \tag{A.6}$$

where the first term is the contributions from the free surface source distribution, the second term is the momentum flux through the control surfaces and the third term is the contribution from inviscid vorticity.

Now we limit ourselves to the x-component of F, F_x,

$$F_x = \rho \sum_i \int\int_{S_i} w_x dS + R_{wo} + \rho \int\int\int_V (w\omega_y - v\omega_z) dV \qquad (A.7)$$

where u, v, w: components of q, $\omega_x, \omega_y, \omega_z$: components of ω and

$$w_x = -\frac{1}{2} n_x q^2 + u q_n \qquad (A.8)$$

$$R_{wo} = -\frac{1}{2}\rho \int\int_{S_\infty} (n_x q^2 - 2u q_n) dS \qquad (A.9)$$

As easily proved, R_{wo} can be given by

$$R_{wo} = \frac{1}{2}\rho \int_{-\infty}^{\infty} dy \int_{-\infty}^{0} dz (\phi_{1y}^2 + \phi_{1z}^2 - \phi_{1x}^2) + \frac{1}{2}\rho g \int_{-\infty}^{\infty} \zeta^2 dy + O(\zeta^3). \qquad (A.10)$$

when the linearized free surface condition is invoked. Eq.(A.10) is familiar form in the linearized wave resistance theory which can be given in terms of the amplitude function of the free wave.

In the first term of Eq.(A.7), we write q in the form of

$$q(x, y, z) = q_i + \frac{\sigma_i}{r^2} n \qquad (A.11)$$

where q_i :velocity excluding the contribution of a source at (x, y, z) and σ_i : the source strength at (x, y, z).
Substituting Eq.(A.11) into Eq.(A.3),

$$\begin{aligned} 2w_x &= -n_x(q_i + \frac{\sigma_i}{r^2} n)^2 + 2(u_i + \frac{\sigma_i}{r^2} n_x)(q_{in} + \frac{\sigma_i}{r^2}) \\ &= -n_x(q_i^2 - \frac{\sigma_i^2}{r^4}) + 2u_i(q_{in} + \frac{\sigma_i}{r^2}) \end{aligned} \qquad (A.12)$$

where q_{in} : normal component of q_i. If the radius of the semi-sphere S_i is taken small enough, the integration of Eq.(A.12) over S_i yields,

$$\rho \sum_i \int\int_{S_i} w_x ds = 2\pi\rho \sum_i u_i \sigma_i \qquad (A.13)$$

Finally we can have

$$F_x = R_{wo} + 2\pi\rho \int\int_{S_F} u' \sigma_F dS + \rho \int\int\int_V (w\omega_y - v\omega_z) dV \qquad (A.14)$$

where u' : u excluding the contribution of σ_F at the integrating position.

The first term of Eq.(A.14) is the linear component, the second is the additional component due to the singularities on the free surface and the last is the contribution of the inviscid vorticity which is the induced drag in our case.

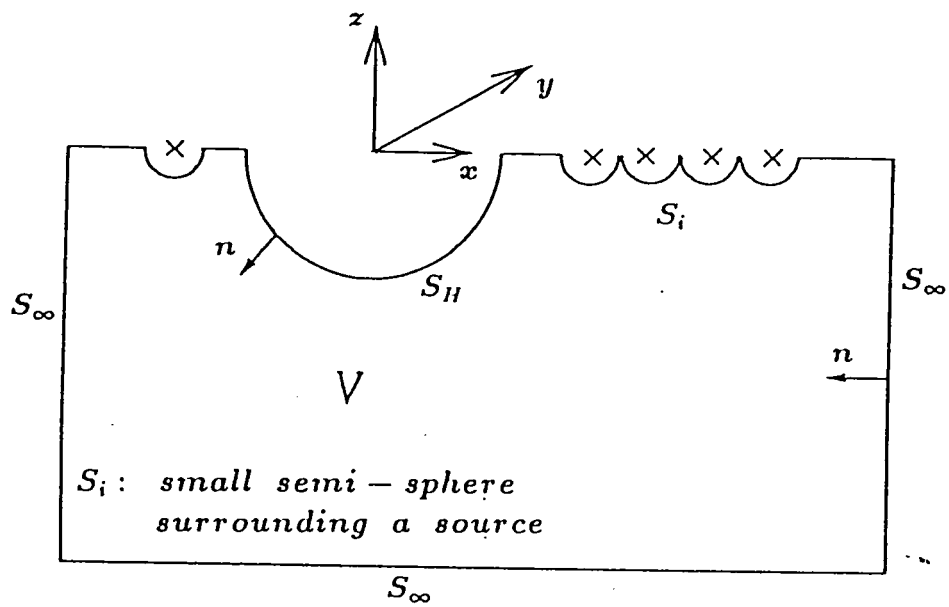

Fig.(A.1) Fluid domain